CHAPTER 11: DIAGNOSTICS

SIEGFRIED SCHREIBER

Deutsches Elektronen-Synchrotron
Notkestraße 85, D-22603
Hamburg, Germany

Keywords

Charge Measurement, Faraday Cup, Toroid, Transverse Shape, Optical Transition Radiation, Wire Scanner, Bunch Length Measurement, Longitudinal Bunch Shaping, Streak Camera, Deflecting Cavity, Electro-Optic Sampling, Beam Position Monitor, Energy Measurement, Energy Spread Measurement, Emittance, Slit Mask Technique, Quadrupole Scanning, Tomographic Reconstruction

Abstract

Understanding the physics of photoinjectors requires accurate and high resolution measurements of its beam properties. In photoinjectors, the beam is bunched. Critical parameters to be measured are the charge of the bunch, its transverse- and longitudinal-size and shape, its emittance, the energy and energy spread, and its position in the accelerator. This chapter gives an overview of the basic techniques in measuring and monitoring the beam properties.

11.1 INTRODUCTION

Photoinjectors produce bunches of electrons that are quickly accelerated to relativistic energies. The injectors often aim for state-of-the art beam properties; for instance, X-ray, free electron lasers (FEL) require a very small emittance and bunches with peak currents at the limit of today's technology. Under these circumstances, measuring the properties of the electron beam is of the utmost importance. The measured data is compared to simulations, and thus provides an essential tool for understanding the underlying physics. In an operating facility, measurements of the beam properties are used to set-up, tune and match the beam optics for further acceleration.

The beam's basic properties are the bunch charge, its transverse- and longitudinal-size and shape, its emittance, energy and energy spread, and its position in the accelerator. In the following chapter, I discuss the most common techniques to measure and monitor these basic parameters. I start with the charge, followed by the transverse- and longitudinal-size and shape, the beam position, and the energy and energy spread. Finally, I discuss measuring the emittance and Twiss parameters. For further reading, I recommend Strehl's comprehensive overview on beam instrumentation and diagnostics [11.1].

11.2 BUNCH CHARGE

Electron beams generated by photoinjectors are bunched. The charge of a single bunch typically ranges from a few picocoulombs to a few nanocoulombs, and the number of electrons roughly 10^9. However, this may vary by orders-of-magnitude depending on the specific application.

RF guns emit dark current. Field emission from surfaces of the gun body or the cathode leads to a spurious current, partly accelerated and detectable on many beam diagnostic devices. Dark current is a background to measurements of electron bunch properties, but also a source of activation of beamline components. In a photoinjector, one would like to know the amount of dark current emitted and accelerated by the RF gun. Novel, non-destructive dark current monitors are in development. An example is a monitor laid out as a resonant cavity operating with the RF frequency of the accelerator. Dark current is bunched with the RF frequency and thus excites a field in the cavity which is measured with suitable pick-up antennas. A

resolution of 40 nC has been achieved. [11.2]. A nice feature of this monitor is that it also measures bunch charges with femtocoulomb resolution. Analyzing the high-order mode signals, an estimate of the bunch length with picosecond resolution is achievable as well.

11.2.1 Faraday Cups

A standard way, and also the simplest one, to measure the charge of electron bunches is with a Faraday cup [11.3]. Faraday cups span a wide dynamic range and are easy to calibrate. They are often used in applications with small bunch charges and are suitable for measuring dark currents, as well.

Figure **11.1** shows an experimental set-up with a Faraday cup to measure charge or current. The cup itself is a metallic structure absorbing the electron beam. It is important that it absorbs all electrons of the bunch, that the electron shower is well contained and that all scattered electrons from the cup (secondaries) are captured. Electrons or ions from showers created elsewhere must not hit the cup. Also, care must be taken to avoid leakage current to the ground.

To contain the shower, the cup has a certain thickness and a geometrical form – typically of a cup – to capture all secondaries. Some designs first use low Z material to avoid backscatter, followed by high Z material, like tungsten or lead, to contain the shower. The Faraday cup is electrically isolated from the beamline and all other components and the electrical connection is made to the measurement device only. In the simplest configuration, the cup is connected *via* a standard 50 Ω cable (for instance, RG58) to an oscilloscope of appropriate resolution, set to an input impedance of 50 Ω. Preferably, the cup should be inside the vacuum system to avoid the passage of electrons through a window generating ions in air.
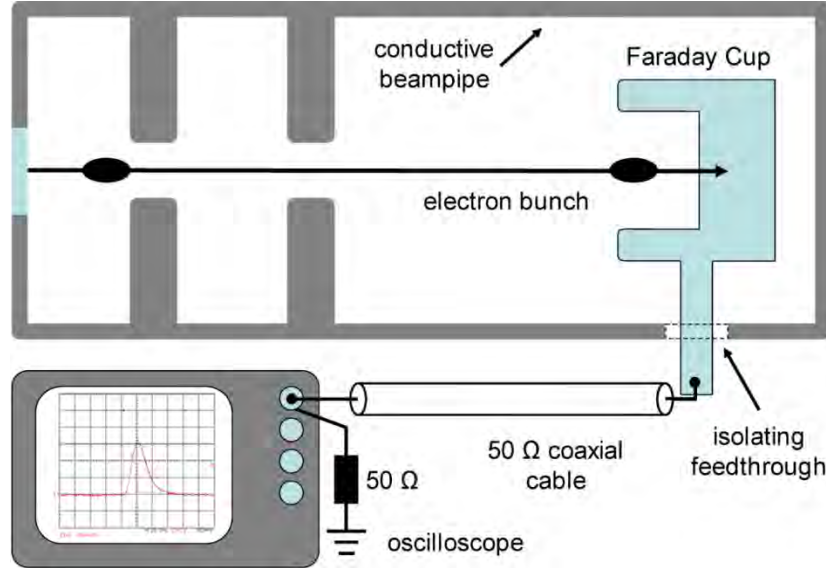

Figure 11.1. Basic set-up to measure the charge of an electron bunch with a Faraday cup. The bunch emerges from the source and passes through some accelerating section before it hits the cup. The cup is electrically isolated from the beam pipe. The current pulse is measured with an oscilloscope terminated to 50 Ω.

The time dependent current of the pulse, $I(t)$, is simply given by

$$I(t) = \frac{U(t)}{R} \tag{11.1}$$

Chapter 11: Diagnostics, S. Schreiber

with the voltage $U(t)$ measured by the oscilloscope with an input impedance of $R = 50 \ \Omega$. The charge is obtained by integrating over the current

$$Q = \int I(t)dt = \frac{1}{R} \int U(t)dt \tag{11.2}$$

The integration is over the duration of the beam pulse and requires careful subtraction of the background. The integration measurement feature of standard oscilloscopes can be used. The background is evaluated by using the same integration measurement set-up, but with the beam switched off.

This procedure gives an absolute measurement of the current or charge with a precision in the 10% range. High precision measurements necessitate more effort: very accurate measurements require special modeling of the cup, especially to avoid backscatter and to contain the shower.

To have a clean pulse and avoid reflections and ringing, the Faraday cup arrangement should also have an impedance of about 50 Ω.

The cup should be inside the beam vacuum, either in a fixed position acting as a beam dump, for instance in a diagnostic section, or mounted on an actuator allowing it to be removed from the beamline when required. For large average currents, the cup may need to be water-cooled. For low energy beams, the weight of the cup still is reasonable and can be handled easily.

The oscilloscope can be replaced by a data acquisition system based on fast analog-digital converters (ADCs) to digitize the output of a sample-and-hold integrator.

The electron bunches in an RF gun are short, typically in the 1-10 ps range, a parameter that must be taken into account in designing the electronics.

11.2.2 Toroids

Faraday cups are destructive devices since they absorb the beam. An elegant way to measure the beam current or bunch charge is by inducing a current in a coil or toroid placed around the beam pipe. The coil acts as a current transformer [11.4]–[11.9] and can be built large enough to fit over the diameter of standard beam pipes. The toroidal design assures that the current- or charge-measurement is independent of the beam position.

Figure **11.2** is a sketch of the type of toroids used at FLASH. In this specific design, two-halves of a torus are clamped together forming a ring. The material is Vitrocvac 6025 [11.10], an amorphous alloy with a high permeability of $\mu_r \approx 10^5$ (for low frequencies of $f < 100$ kHz) and a high electrical resistance for a fast decay of Eddy currents [11.11]. At higher frequencies, the permeability decreases like $\mu_r \propto 1/f$.

The clamped design offers the nice advantage of allowing mounting and removing of the toroid without opening the beam vacuum.

A small ceramic ring mounted into the beam pipe breaks the electrical contact, allowing the field of the electron bunch to interact with the toroid. The wall current, which normally flows along the pipe, is now guided around the toroid's housing with a low impedance bypass. Figure **11.3** is a 3-D model of a toroid used at FLASH and at the European XFEL.
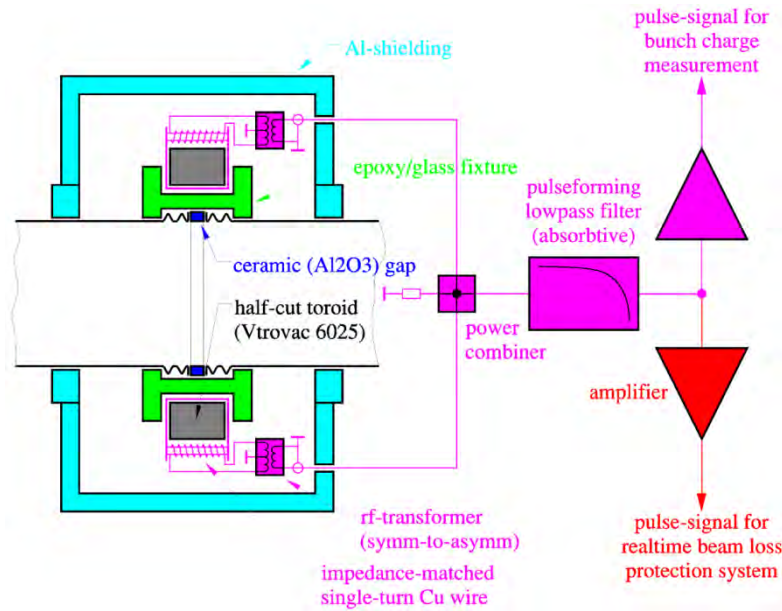
Figure 11.2. Sketch of a toroid system with read-out. The transformer coil (gray) is placed around the ceramic gap (dark blue). In this design, two quarter torus pieces of Vitrovac 6025 [11.10] are clamped together, each having its own readout. The signals are combined and distributed to the read-out system. One branch is used for charge measurements and one to measure beam losses between adjacent toroids. [Courtesy of M. Wendt, FNAL]
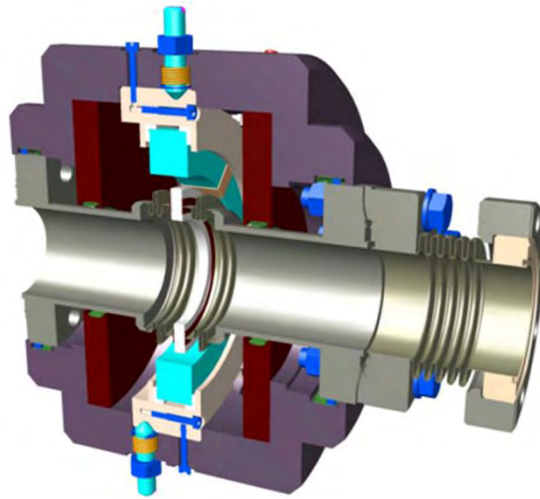

Figure 11.3. Toroid assembly at FLASH and the European XFEL. The drawing shows a cut out of the toroid's housing and the vacuum chamber. The transformer coil (cyan) is visible over the ceramic gap (white) that is welded into the vacuum chamber. The housing (violet) serves as a shield and a bypass for the wall current. Read-out connectors also are shown. [Courtesy of M. Siemens, DESY]

The ceramic gap may be metalized to avoid charging up. This especially is advisable for RF guns with a high level of dark current. In this case, the impedance of the bypass must be much smaller than the impedance of the metallization.

For low charges, amplifiers must be mounted close to the toroid. Typically, the analog signal is transported with a 50 Ω cable to the data acquisition system.

In contrast to Faraday cups, toroids must be calibrated because the transformer ratio and the amplifier gain may not be known exactly. In fact, calculating the transformer response is rather complex. Here, the reader is referred to Strehl's book [11.1] and the JUAS lectures given by Forck [11.11].

Chapter 11: Diagnostics, S. Schreiber

Following Strehl's evaluation of a passive transformer – without an additional amplifier – the voltage response $U(t)$ is given approximately by

$$U(t) = -I_p \frac{R}{N_w} e^{-t/\tau_d} \qquad (11.3)$$

The beam current, $I(t)$, is idealized to a step function with a peak current of I_p. This simplified model yields us some basic properties of a toroid transformer. The output voltage is proportional to the inverse number of windings $U \propto N_w^{-1}$. In contrast, the transformer inductance L is proportional to $L \propto N_w^2$. The sensitivity S, defined as the ratio of the output voltage to the beam current, is given by

$$S = \frac{U(0)}{I_p} = \frac{R}{N_w} \propto \frac{1}{N_w} \qquad (11.4)$$

and the droop time constant τ_d, of the exponential voltage droop is given by

$$\tau_d = \frac{L}{R_L + R} \approx \frac{L}{R} \propto N_w^2 \qquad (11.5)$$

where R is the load resistance of the system, and R_L is the resistance of the cables in the secondary circuit, which is usually much smaller than R.

For a good low frequency response and a large droop time constant, the number of windings N_w should be high. On the other hand, for good sensitivity or voltage response, the number of windings should be low. However, using operational amplifiers, the large load resistance is overcome so that the droop time due to the very small R_L is considerably increased with $\tau_d \approx L R_L^{-1}$ (Equ. 11.5) without needing to increase N_w, thus allowing one to choose a rather small number of windings to attain good sensitivity.

Evaluating the rise time, τ_r, of the output signal for high frequencies involves taking into account the stray capacitance, C_s, and the stray inductance, L_s. The former is caused by the capacitance between the windings, the windings and the toroid, as well as the cables. The inductance of the toroid decreases due to the decreasing permeability with $1/f$. For frequencies ~100 MHz, the stray inductance becomes the dominant contribution [11.11]. τ_r is given by

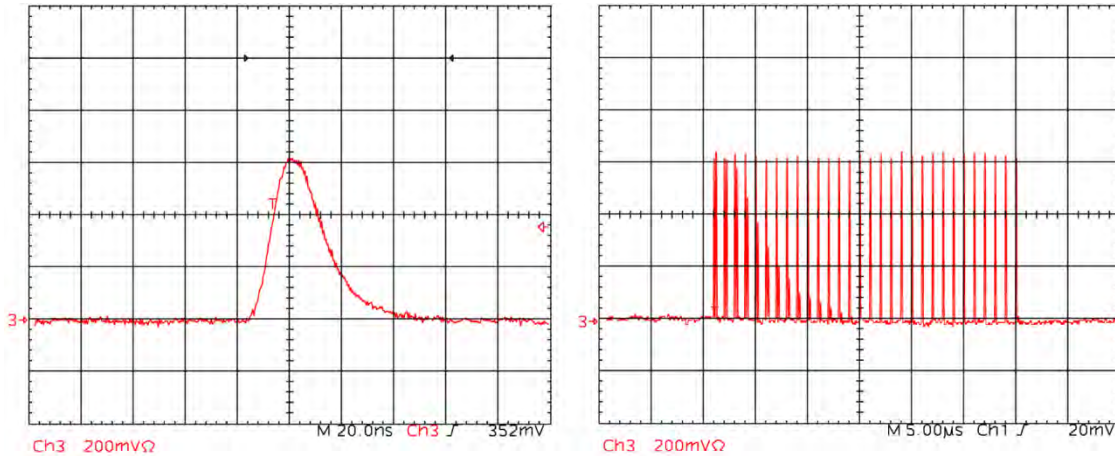$$\tau_r = \sqrt{L_s C_s} \qquad (11.6)$$

The rise time is defined the same way as is the droop time in Equ. 11.3,

$$U(t) \propto (1 - e^{-t/\tau_r}) \qquad (11.7)$$

With a typical stray capacitance and inductance, the rise time is on the order of nanoseconds: this is independent of the pulse duration of the electron bunch, which is in the picosecond range. The left of Figure **11.4** shows an example of a voltage output signal of an electron bunch. Here, the length of the voltage pulse is 20 ns, the length of the electron bunch is only 10 ps, and the bunch charge is 1.2 nC.

Calibrating the toroids is straightforward. A pulse of a known charge is fed through a loop around the coil and the coil response is measured. For instance, a temporally rectangular pulse generated by a standard pulse generator with a length of 50 ns and a voltage of 1 V terminated with 50 Ω has a charge of 1 nC. The calibration constant is obtained by integrating the resulting voltage pulse, very similar to in the case of the Faraday cup (Equ. 11.2 in Section 11.2.1). The beam charge is then measured by integrating the toroid current pulse and applying the calibration constant. A standard 500 MHz scope terminated to 50 Ω can be employed, or better, a suitable data acquisition system with a sample-and-hold integration. As discussed above, the shape of the output pulse is independent of the electron pulse. For simplicity, it is possible to measure the peak voltage only, omitting the integration.

Many photoinjectors produce pulse trains. FLASH, for instance, has trains of hundreds of individual pulses with 1 µs spacing between them. The right of Figure **11.4** shows an example of a pulse train of 30 bunches. For pulse train durations comparable to the droop time constant τ_d (Equ. 11.5), the voltage droop from pulse to pulse must be accounted for. A typical droop is about a few percent per microsecond.

Figure 11.4. Examples of toroid signals measured with an oscilloscope. The voltage response of a single electron bunch (left), and of a train of 30 bunches with a spacing of 1 µs (right). Although the duration of the bunch is 10 ps, the width of the voltage response of a single bunch is 20 ns. A small voltage droop along the bunch train is visible. The bunch charge in this example is 1.2 nC (vertical scale 200 mV per division, horizontal scale 20 ns (left) and 5 µs (right) per division and a termination of 50 Ω).

To correct for the droop, the signal height is measured as the difference between the peak voltage and the baseline. Each pulse in the train is sampled at its peak and at the baseline, close to the pulse (a few nanoseconds earlier).

Care must be taken with external magnetic fields that may saturate the toroid. Vitrovac 6925, for instance, saturates at 0.58 T. [11.10] RF gun designs use large, strong solenoids to compensate for the space charge induced emittance growth. The toroid should be mounted at an appropriate distance from the solenoid.

For good toroid designs, the linearity of the charge measurement is better than 10^{-4} with a resolution on the order of 1 pC in a wide dynamic range.

11.3 TRANSVERSE SHAPE

A good knowledge of the transverse bunch shape at various locations along the injector beamline is mandatory for tuning the injector for a small transverse beam emittance and for matching the beam optics to the accelerator's optical design. This section details the measurement of the transverse shape: measuring the emittance is covered in Section 11.7.

A transverse image of the beam usually is obtained by letting the electron beam hit a screen that in turn emits photons in the visible wavelength spectrum. The emitted light is guided out of the beam pipe through a window and imaged by an appropriate imaging system on a high resolution detector. Nowadays, commercial CCD cameras with suitable optics (objectives or lenses) provide the required magnification and resolution.

Another method to determine the transverse shape is based on using thin metallic wires hit by the electron beam, for example, a fine grid of several wires or a so-called wire scanner, which is a single wire moving through the beam. Either the electrons scattered by the wire or the current induced by it is measured as a function of the wire's position. The wire scanner provides a 1-D, averaged projected profile of the beam. It has the advantage of being almost non-destructive and is a fast measurement of the beam size. In contrast, although wire grids are destructive, they yield a single shot 2-D charge distribution. However, they are rarely used since it is easier to realize a screen system with an excellent resolution of 10 μm.

11.3.1 Screens

The simplest method to measure the transverse bunch shape and size is to use a screen in combination with a suitable imaging system, which could be a simple commercial objective, or a more dedicated set-up of several lenses and other optical components. In most cases, the images are recorded by a commercial CCD camera.
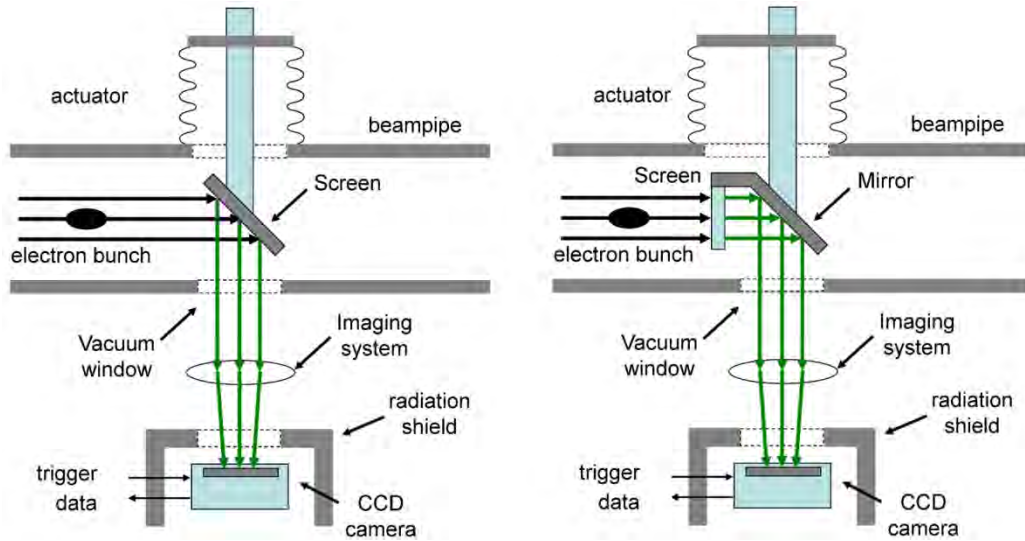
Most screen monitors use flat screens made of scintillating, fluorescent material or having a polished metallic surface (in the case of optical transition radiation), inserted at an angle of 45° with respect to the beam. The backward radiation emitted from the screen is guided out of the beam pipe through a window and transported into the imaging system. The vacuum window should be radiation hard to remain transparent in the range of optical wavelengths for a long time; windows made out of the best quality fused silica are an example. To reduce γ-radiation hitting the camera, an additional 45° mirror often is used in the optical system. Figure **11.5** is a sketch of a typical set-up.

The simple arrangement described works for most applications. For high resolution measurements, care must be taken to polish the optical transition radiation (OTR) screens to optical quality. For fluorescent or scintillating screens, other factors may influence the resolution, such as grain size, crystal thickness, orientation angle with respect to the beam and the camera, and the choice of optics.

The depth-of-focus effects need to be considered only when a very high resolution for large spot sizes is required. For screens mounted at 45° with respect to the beam, this effect may limit the resolution since radiation created on the screen from different parts of the beam have different distances to the CCD of the camera, and thus are imaged differently. The beam image itself is not distorted. Since the electrons are moving almost at the speed of light, the screen acts like a normal mirror. To retain the best resolution, it is also important that the beam hits the point of the screen for which the imaging system was adjusted, usually the center.

When the screen is placed normal to the electron beam, the path length of the radiation is equal over the entire bunch. However, the set-up then is more complicated: a mirror is required to guide the emitted photons out of the beam pipe. Figure **11.5** illustrates an arrangement using forward radiation from an optically transparent crystal. Also, a screen coated on the back side with a material emitting the radiation can be employed.

Figure 11.5. Typical set-up of a screen system to measure the transverse shape of an electron beam. A standard system uses a flat screen with fluorescent material or a polished metallic surface for optical transition radiation at an angle of 45° with respect to the beam (left). An optical system images the screen surface onto a CCD camera. A system avoiding the depth-of-focus issue places the screen normal to the electron beam direction (right). In this arrangement, the screen is either optically transparent or the radiation is created at the back surface to allow imaging over an additional mirror (here shown with an angle of 45°). In both versions, the screen and mirror are retractable from the beamline.

For this type of set-up, a complication occurs when coherent optical transition radiation has to be considered. Such radiation is also emitted in the forward direction by the radiator and the backwards direction by the mirror. Interference between the two sources will be visible, complicating the analysis of the image. The interference pattern depends also on the beam energy, since the slippage between the two radiation sources is given by the difference between the speed of light and that of the electrons. Special experiments were undertaken to measure this effect [11.12], [11.13]. In practice, where coherent optical transition radiation is not expected, the number of photons from high efficiency radiators is considerably larger than the number of photons emitted by optical transition radiation, so this effect can be neglected.

The screen typically has a size of approximately a centimeter and can be moved in and out of the beam pipe, either by pneumatic actuators or motorized drives. Motorized actuators are used when several different screens mounted on a single actuator must be inserted. The actuator has end switches and intermediate position sensitive switches to insert the different screens properly. In machines with a large number of high charge bunches per second, the switches are also used by the machine protection system to prevent damaging the screens. The number of bunches allowed is limited when the screen is inserted.

Transverse bunch sizes in a typical injector are in the millimeter scale; for higher beam energies, they are on the order of 100 μm. Even smaller sizes, some tens of micrometers, are obtained, for instance, during solenoid scans. Measuring the beam size as a function of the RF gun solenoid field is a typical measurement to validate simulation codes.

The applied optical system must take into account the expected size of the beam. Typically, a screen monitor system should be able to measure bunch sizes down to 50 μm, or even less. A good system should aim for a resolution on the order of 10 μm. For some cases, a simple system with a commercial objective will suffice. Others may require a more complicated and flexible system. The optical elements should always be of high quality: achromatic lenses are used, and suitable apertures may be needed to reduce chromatic aberration. Retractable neutral density filters adjust the light intensity to avoid saturating the CCD camera. Wavelength filters to select a specific spectral range are sometimes included.

The pixel size of a standard CCD camera with a ½-inch sensor is about 10 μm × 10 μm. The rms resolution, σ_p, of a pixel sensor of size, l_{pix}, is limited to

$$\sigma_p = \frac{l_{pix}}{\sqrt{12}} \qquad (11.8)$$

Here we assume, that always several pixels are hit by the beam, so that the rms beam size σ_x in one transverse direction[1] can be determined using the second moment of the distribution

$$\langle x^2 \rangle = \frac{\sum_{i=1}^{n} W_i \, (x_i - \langle x \rangle)^2}{\sum_{i=1}^{n} W_i} \qquad (11.9)$$

with $\langle x \rangle$ being the first moment defined by

$$\langle x \rangle = \frac{\sum_{i=1}^{n} W_i \, x_i}{\sum_{i=1}^{n} W_i} \qquad (11.10)$$

The sum is taken over all pixels in a certain row or column indicated by $i = 1 \ldots n$, x_i is the transverse coordinate, and W_i the number of counts of pixel i. A beam with a size less than one pixel appears as one pixel only and cannot be resolved with a resolution better than the pixel size.

The transverse coordinate is calculated from the pixel number by applying a calibration constant such that $x_i = ki$. The calibration constant k is given by the pixel size l_{pix} and the magnification M of the optical system where $k = l_{pix} \, M^{-1}$. Since neither the pixel size nor the magnification is known exactly, the calibration constant is obtained using special marks on the screen with a known distance or with special calibration screens. A remotely controlled light source to illuminate the calibration marks eases the calibration procedure and should be included in the design of the screen station.

The counts in each CCD pixel are proportional to the number of photons hitting this pixel, which, in turn, is proportional to the charge of this specific part of the beam. To obtain a projected size, the pixel counts in one row or column are summed up first.

Using the second moment, the rms beam size is given by

$$\sigma_x = \sqrt{\langle x^2 \rangle} \qquad (11.11)$$

Care has to be taken to correctly subtract the background. The second moment is sensitive to spurious pixel counts far from the beam center. High pixel counts created, for instant, by broken pixels or γ-rays need to be eliminated. A background image is usually taken under the same condition as with beam, but the beam is

---

[1]The coordinate system used is left-handed Cartesian, with the horizontal coordinate x, positive to the right in beam direction, the vertical coordinate y, positive up, and z pointing in the direction of the beam. In order to simplify the notation, we use x, even though a similar relation holds for y, as well.

switched off. This is best done by blocking the drive laser of the RF gun while keeping all other parameters the same.

Figure **11.6** is an example of the profile of a transverse beam measured using optical transition radiation with a CCD camera.

Usually, the shape of the beam is not Gaussian. However, if it is close to a Gaussian distribution, a fit to a Gaussian function can be used to determine the beam size. In this case, the rms beam size is equal to the standard deviation σ of the Gaussian function.

A prerequisite to achieving a resolution below 10 µm with a standard CCD camera is that the magnification of the optical system is at least $M = 1$. However, not only does the pixel size limit the resolution of the system, but also the properties of the whole optical system.

With a magnification of 1, it is often impossible to image the whole screen onto the CCD sensor. Let us take, as an example a CCD sensor having 658 × 494 pixels with a pixel size of 10 µm × 10 µm (a typical ½-inch sensor). With a magnification of 1, an area of 6.6 mm × 4.9 mm is imaged, the size of the CCD chip. Assuming a screen with dimensions of 20 mm × 20 mm, a magnification of 0.3 would be required to image the whole screen. Therefore, many screen systems have arrangements with multiple magnifications. Figure **11.7** shows a system with three magnifications [11.14]. Three magnifications, 1, 0.39 and 0.25, are realized with three different lenses, which are remotely movable into and out of the optical pass.
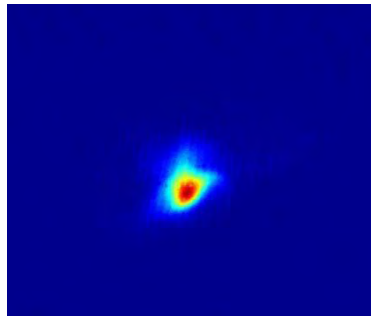

Figure 11.6. Example of an image of an electron beam taken with an OTR screen at FLASH. The beam size in this example is 200 µm rms. The false colors encode the pixel count: Blue is very low, green to yellow is increasing and red represents high pixel counts. The pixel count is proportional to the numbers of photons hitting a specific pixel.

Commercial digital CCD cameras are used nowadays. The camera is connected to a computer where the read-out software is running, for instance, with an IEEE 1394 interface, an Ethernet connection, or by other means. A beam signal triggers the camera. The control system provides an online image of the electron beam. Beam profiles and sizes are determined from the recorded images by dedicated image analysis software.

The exposure time of standard digital camera is several microseconds. Therefore, obtaining single shot images of the electron bunch is possible only for machines with low repetition rate or with specially designed fast cameras.

To obtain single shot images of high repetition rate bunch trains, gated intensified cameras are used. Compared to standard cameras, they are expensive and use image-intensifiers based on a photocathode together with a micro-channel plate to amplify the electron signal. The electrons then are back-converted to

Chapter 11: Diagnostics, S. Schreiber

light using a phosphor screen and subsequently imaged by a CCD camera. This set-up allows nanosecond scale gating of the electron signal, opening the possibility for measuring a single bunch in bursts of bunches, where individual ones are only a few nanoseconds apart. I note that the number of bunches with a given charge and size allowed to hit a screen is limited by the damage threshold of the coating on the screen or the screen material itself.

The properties of the screen monitor considered above do not depend on the choice of the screen type: the set-up is similar for both, fluorescence screens and for screens producing OTR. These two types of screens have special characteristics which need to be considered when choosing a screen suitable for a specific application.
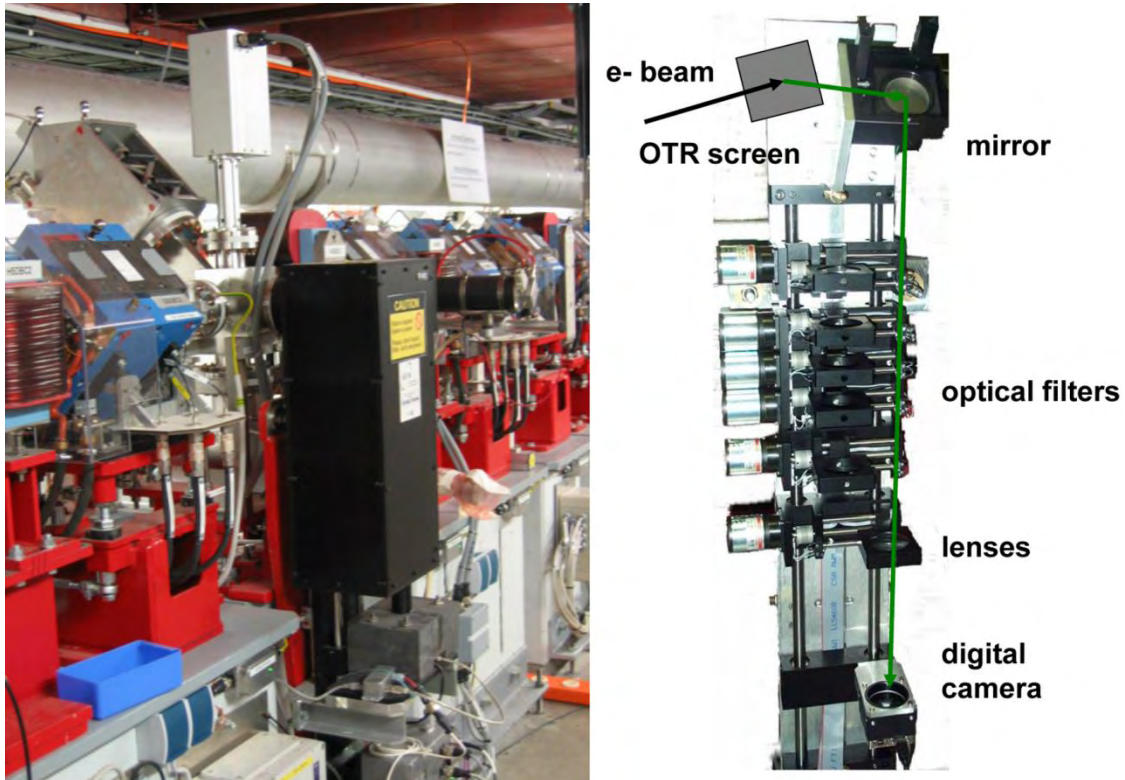

Figure 11.7. OTR screen system of FLASH. The picture on the left shows the system as installed at FLASH; on the right, the cover was removed to reveal the optical system with optical filters (attenuators), lenses and the CCD camera. On top of the beamline, the actuator that moves screens into the beam is visible. Two different screens and a calibration screen can be placed in the beam path. Three remotely controlled lenses allow one to choose between three different magnifications, optical filters and attenuators. A commercial digital CCD camera [11.15] with a pixel size of 9 μm × 9 μm is used. The resolution of the measurement of the beam size is 11 μm.

11.3.2 Fluorescence Screens

Scintillators or fluorescent screens[2] are an appropriate choice for measuring beam size at energies $\ll 50$ MeV, or when a high photon yield is required.

Earlier, scintillators of zinc sulfide or activated plastic were the standard screen material. However, they frequently exhibited damage due to radiation. A radiation-hard material was developed in the late '60s, *i.e.*,

---

[2]I do not explicitly distinguish between scintillation and fluorescence. Scintillators emit light when particles transverses the material; fluorescence occurs when photons excite the material's atoms, which decay back to the ground level. Particles in an electromagnetic shower like electrons, photons, and positrons emit light through many processes not detailed herein.

chromium activated aluminum oxide scintillators. [11.16] A subsequent step forward was the introduction of alumina ceramic fluorescent screens at CERN (Chromox-6). [11.17] Chromox is a commercial material, but was developed with collaboration with CERN. [11.18] For low charge bunches and where a strong photon signal is required, this type of screens is a suitable choice. It is a robust aluminum oxide, ceramic-doped with chromium oxide for ultra-high vacuum applications (typically 99.4% Al_2O_3 and 0.5% Cr_2O_3). A typical plate is 1 mm thick, with a favorable grain size of 10-15 μm. The fluorescence lifetime at room temperature is 3 ms. [11.17] The light yield depends on the thickness of the plate; a 1 mm thick plate gives enough light for a beam with about 10^9 electrons per square-centimeter. Chromox may saturate and therefore is not suitable for high precision measurement of bunches with a high charge density; and due to the long fluorescence lifetime, they are not used for high repetition rate beams either.

Ce:YAG, Yttrium aluminum oxide crystals doped with, for instance, Cerium (1%) has been proven to be linear in a wide charge density range [11.19] with a fast decay time and therefore is typically applied at RF gun photoinjectors. Commercial Ce:YAG crystals are available at a size of about 1 cm × 1 cm and a couple hundred of micrometers thick. The crystal is transparent and is usable in both configurations shown in Figure **11.5**. Table **11.1** lists basic properties of Ce:YAG.

Property [units]	Value
Index of Refraction	1.82
Wavelength of Peak Emission [nm]	550
Density [g/cm^3]	4.55
Radiation Length [cm]	3.6
Photon Yield [photons per MeV]	8×10^3
Cerium Concentration [with respect to Yttrium]	0.18%
Decay Time [ns]	70

Table 11.1. Basic properties of Ce:YAG. [11.20], [11.21]

Saturation at high charge densities is an issue for Ce:YAG, as well. Comparison with data from OTR and wire scanners show that Ce:YAG saturates at 0.01 nC μm^{-2}. [11.20] Besides the depth of focus problem described above, the optical resolution is limited by the crystal's thickness and light reflection from its back surface.

11.3.3 Optical Transition Radiation

Transition radiation is produced whenever a charged particle passes through a surface of any material. The transition between two media with different dielectric properties forces the electromagnetic field of the electron to adapt to the properties of the new media. The difference in the fields is emitted as transition radiation in the forward and backward directions with respect to the boundary surface. The forward radiation is emitted in the direction of the electron beam trajectory and the backward radiation in the direction of the specular reflection (Figure **11.8**).

The angular distribution of transition radiation is energy dependent: it peaks at an angle of θ_{peak}

$$\theta_{peak} = \frac{1}{\gamma} = \frac{E}{m_e c^2} \qquad (11.12)$$

where γ is the relativistic factor, E is the electron energy, m_e the electron mass and c the speed of light.

At ultra relativistic energies and assuming a perfectly reflecting metallic surface, the photon intensity per solid angle and per unit frequency emitted by a single electron with charge e is approximated by a simple expression

$$I(\theta,\omega) = \frac{e^2}{(4\pi\varepsilon_0)\ \pi^2 c} \frac{\theta^2}{(\gamma^{-2} + \theta^2)^2} \tag{11.13}$$

where e is the electron charge magnitude and ε_0 the permittivity of free space. The angle θ is defined with respect to the direction of specular reflection for the backward radiation, and with respect to the electron beam trajectory for the forward radiation (Figure **11.8**). Equ. 11.13 is valid for $\gamma \gg 1$ and $\theta \ll 1$.

Figure **11.8** illustrates the angular distribution of transition radiation emitted by an electron with an energy of 1 GeV. Although the distribution peaks at an angle of $\theta_{peak} = \gamma^{-1}$, due to the long tails, a large part of the photons are emitted at angles significantly larger than θ_{peak}.
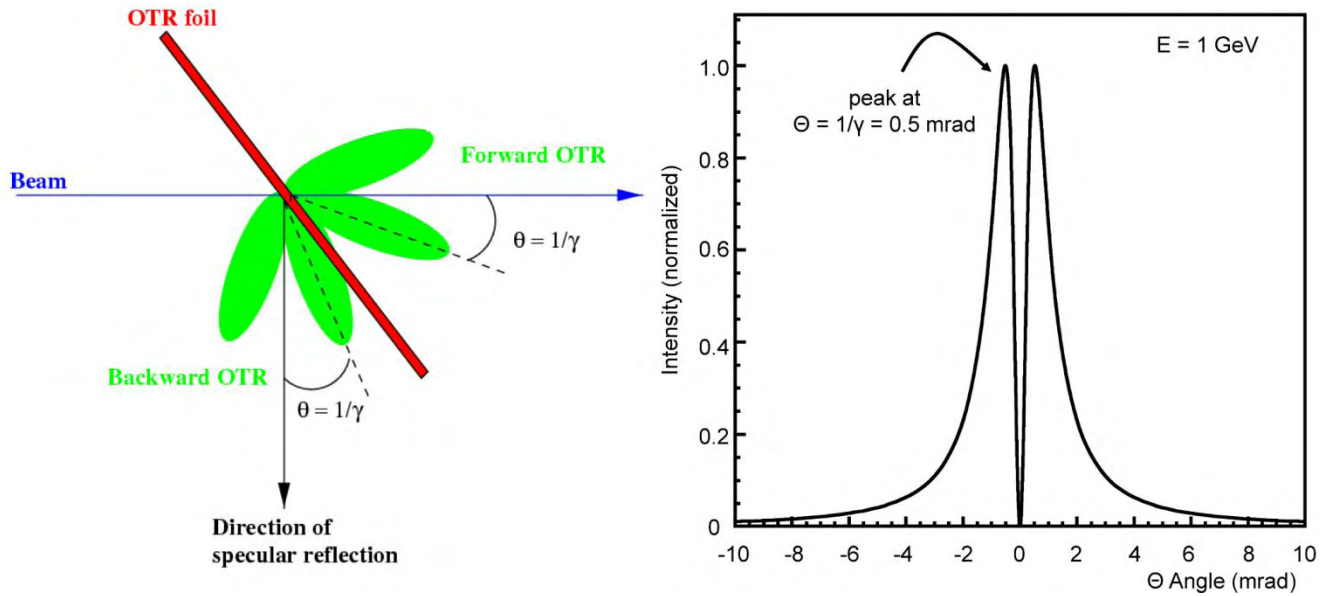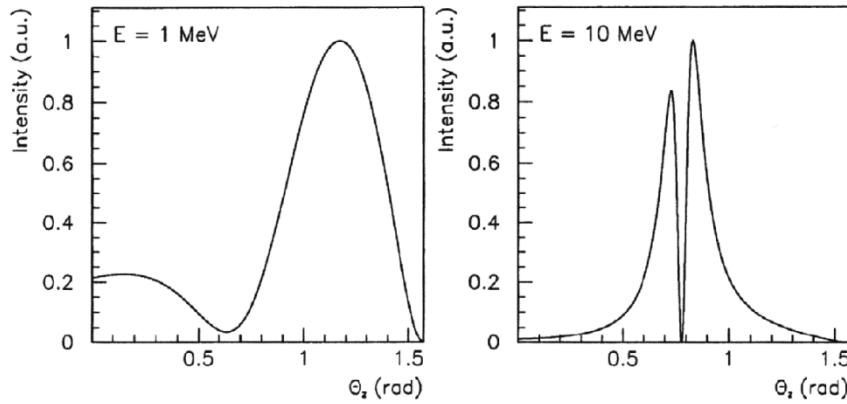

Figure 11.8. Optical transition radiation (OTR) produced when an electron beam traverses a medium; here, a plane metallic foil is shown (left). The radiation is emitted in the forward direction (the direction of the beam trajectory) and in the direction of the specular reflection (backward). The angular distribution of OTR reveals a ring-like structure peaking at $\theta_{peak} = 1/\gamma$ (right). The distribution shown was calculated for a beam energy of 1 GeV. [Courtesy of K. Honkavaara, DESY] [Adapted from [11.22], with permission from Elsevier]

For non-relativistic energies, $\gamma \approx 1$, as is the case for RF guns, a more complicated formula for the angular distribution applies [11.23]. In this case the distribution is asymmetric. Figure **11.9** shows the angular distribution for $E = 1$ MeV and $E = 10$ MeV. In both cases, the screen is tilted by 45˚ with respect to the beam direction.

Transition radiation has a wide spectrum, but typically the visible wavelengths (OTR) are used when measuring the transverse size and shape of an electron beam. In the optical wavelength range, standard commercial high resolution CCD cameras are available.

The advantages of OTR are its linear response to the electron beam charge and its fast response time, supporting single shot measurements. Also, the measurement set-up is quite simple: typically, a metallic,

thin, flat, mirror-like screen with optical quality is used as a radiator target. For example, a 300 μm thin silicon wafer coated with aluminum is a suitable choice. Figure **11.6** is an example of an image of an electron beam using an OTR system at FLASH.

Figure 11.9. Angular distributions of optical transition radiation for low energy electrons, 1 MeV (left) and 10 MeV (right). The screen is tilted by 45° with respect to the beam direction. In contrast to high energies, the angular distribution is asymmetric. [Courtesy of K. Honkavaara, DESY]

OTR is a standard method used for beam imaging at high electron beam energies. However, for low beam energies (below ~50 MeV), the number of photons emitted may be insufficient for high resolution imaging of the electron beam's transverse shape with standard optics.

The number of photons emitted per electron, N_γ, in the frequency band $[\omega_1, \omega_2]$ is on the order of the fine structure constant, $\alpha = e^2 \, (4\pi\varepsilon_0\hbar c)^{-1} \approx 1/137$, and increases logarithmically as a function of the electron energy

$$N_\gamma = \frac{2\alpha}{\pi}\left(\ln(2\gamma) - \frac{1}{2}\right)\ln\left(\frac{\omega_2}{\omega_1}\right) \tag{11.14}$$

At an electron beam energy of 10 MeV, about 100 electrons are needed to emit a single photon in the optical wavelength range ($\lambda = 350\text{-}750$ nm). As considered above, the OTR angular distribution depends on the electron energy: the smaller the beam energy, the wider is the distribution. The angular acceptance of a typical screen monitor is about a couple hundred milliradians. Therefore, at low energies, it often is practically impossible to transport enough photons to a standard CCD camera.

Then, fluorescent screens, as discussed in the previous section Section 11.3.2, should be chosen.

11.3.4 Wire Scanners

Wire scanners are expensive and technically demanding devices. Their disadvantage compared to screens is that the wire is scanned through the beam giving an average projected profile, not a single shot 2-D image. For this reason, wire scanners are applied only if the technology is at hand, or where they are indispensable. There are a number of examples where wire scanners are successfully used for high repetition rate accelerators, like the SLAC linac SLC, LEP at CERN and others [11.24]–[11.27]. Wire scanners are also applicable where the coherent effects of OTR hamper the proper analysis of screen images, such as LCLS and FLASH.

A wire scanner consists of a thin wire, typically tungsten or carbon that is moved through the electron beam. Usually the radiation scattered off the wire is measured with a suitably placed scintillator and read-out with a photo multiplier. The thickness of the wire should be less than the expected beam size. A typical thickness is 10 or 30 μm. The response of the read-out system to a given charge hitting the wire has to be accounted for. The wire is mounted on a fork, which is moved with a motorized system, as illustrated in Figure **11.10**.
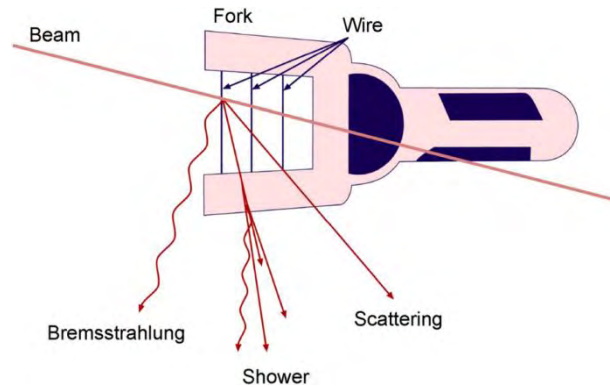

Figure 11.10. Sketch of wires mounted on a fork. Scattered radiation is measured while the wire moves through the beam. [Reprinted from [11.27] with permission from Elsevier.]

The wire's position is measured with precise encoders. The step size or the encoder's resolution should be a small fraction of the beam size. Typically, a resolution of 10 μm is obtained. In some systems, the fork has wires mounted horizontally, vertically and also at an angle of 45˚. Such systems can measure the horizontal- and vertical-profile together with a possible correlation at the same scan. Figure **11.11** has examples of wire scans in the FLASH undulator.
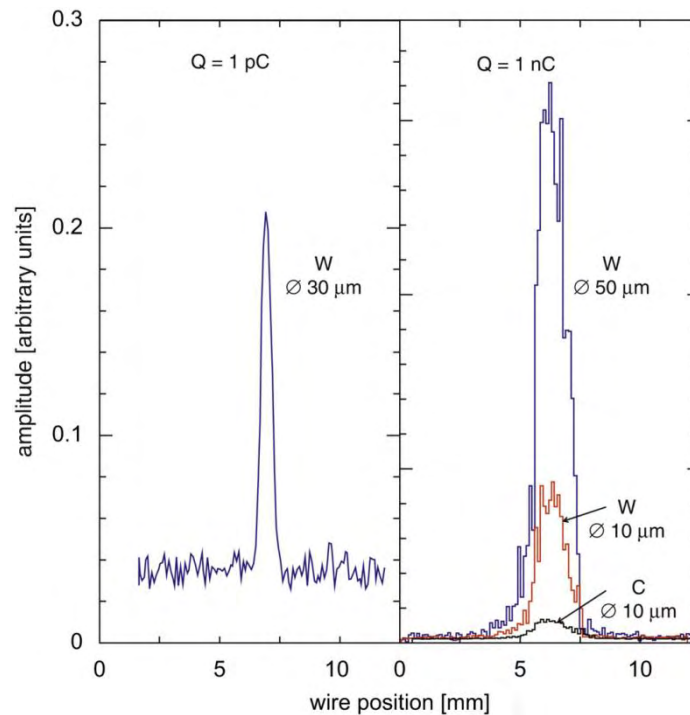

Figure 11.11. Example of several wire scans of the electron beam at FLASH in the undulator section. While the wire is scanned through the beam, signals from the scintillator panels are recorded. Scans are shown for tungsten wires with varying diameters for a very small (1 pC) and normal bunch charge (1 nC). A scan with a 10 μm carbon wire is also shown. [Reprinted from [11.27] with permission from Elsevier.]

For all wire scanner systems, care must to be taken to avoid breaking the wire, for example due to heating by the electron beam [11.28] or mechanical stress. Also, vibrations of wires during fast scans must be considered and damped. [11.29]

11.4 BUNCH LENGTH MEASUREMENTS AND LONGITUDINAL BUNCH SHAPE

Another important electron beam parameter is the bunch length and its shape. A typical bunch length at the RF gun is on the order of millimeters, corresponding to durations of a couple of picoseconds. In some applications, shorter bunches are realized down to the 100 fs scale. In FELs, the bunch is compressed to tens of micrometers to achieve the required peak current in the kiloamperes range. Compression usually is obtained *via* magnetic chicane bunch compressors.

Determining longitudinal bunch properties is more complicated than measuring transverse ones. A direct time resolved measurement requires ultrafast detectors and devices that are not readily available. Often the longitudinal phase space is transformed into the transverse phase space allowing the use of standard methods like screens viewed with standard cameras.

Most methods use incoherent and coherent radiation produced by the electron beam, for example, streak cameras and interferometers. This radiation can be synchrotron radiation that is emitted when the electron bunch moves along a curved trajectory, *e.g.*, through a bending dipole magnet. At beam energies above 100 MeV, synchrotron radiation is emitted in the optical wavelength range required for streak cameras. Another approach is to use transition or diffraction radiation; this is useful for beam energies above 25 MeV. The former is emitted when the beam passes through a screen and the latter as the beam travels through an aperture, for instance a slit. OTR is discussed previously in Section 11.3.3. For beam energies below 25 MeV, Cherenkov radiation can be used, which is generated when a particle travels inside a medium wherein the speed of the particle exceeds the velocity of light. Aerogel with a very low refractive index, or Sapphire with its very high refractive index, are used as Cherenkov radiators.
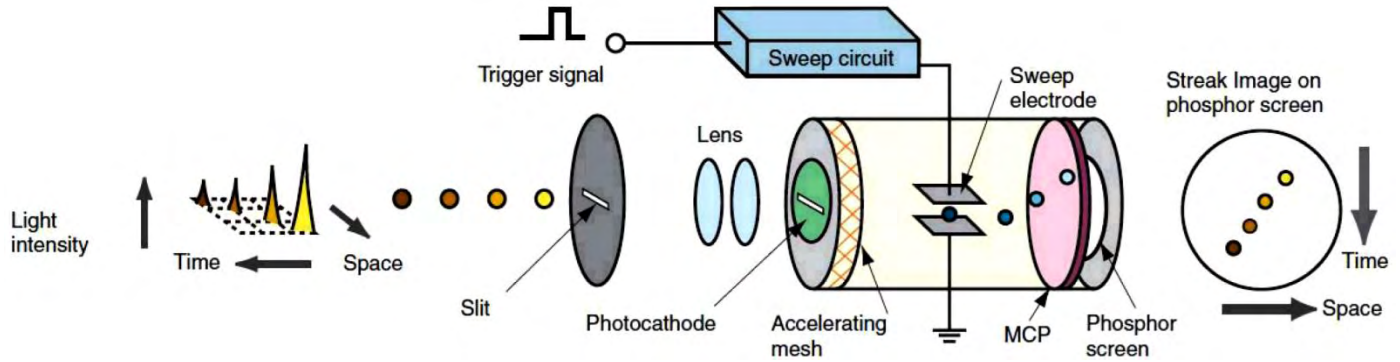
An example of directly measuring the electron bunch length in the time domain is the transverse deflecting RF structure. Here, the beam is streaked by an RF field. The longitudinal charge distribution in the bunch is mapped onto a transverse screen and imaged with standard imaging methods. A deflecting structure can serve for all beam energies.[1]

11.4.1 Streak Camera

The streak camera provides a convenient way to measure electron bunch lengths in the millimeter and sub-millimeter range. The method is based on the prompt emission of light in the optical wavelength range, for instance OTR (see Section 11.3.3), synchrotron radiation [11.30], or Cherenkov radiation [11.31]. An important feature is that the light pulse is a "replica" of the longitudinal shape of the electron pulse. Suitable optics guide the light pulse to the streak camera. Pulse broadening due to diffraction effects must be avoided. In the streak camera, the incident light is passed through a narrow slit and is then converted into photoelectrons by a high efficiency photocathode, like S-20. The electrons are accelerated and deflected transversally by a streak tube applying a fast linear deflecting field. Typically, a streak speed of 2-5 ps mm^{-1} is obtained. The deflection is proportional to the arrival time of the electrons, and thus, to the time structure of the incident light pulse. A phosphor screen (P-20) including an image intensifier converts the streaked electrons back to photons that are finally imaged to a CCD chip of a high resolution, low noise camera. Figure **11.12** shows the principal features of the layout of a streak camera.

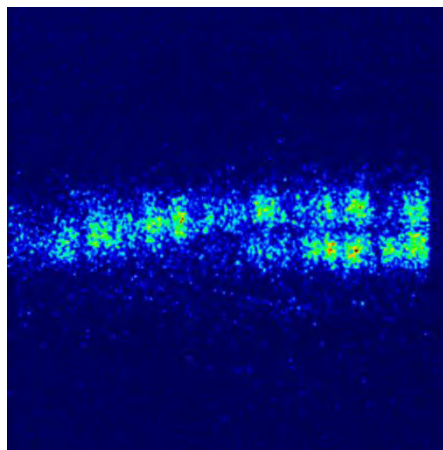[1]At the high energy end of several gigaelectron volts, a deflecting structure may be inappropriate.

Figure 11.12. Principal layout of a streak camera. The light passes through a narrow slit and is then converted into photoelectrons by a high efficiency photocathode. The electrons are accelerated and deflected transversally by a streak tube. The streaked electrons are converted back to photons by a phosphor screen and amplified by an image intensifier. Finally, the image is recorded by a CCD camera. [Figure from [11.32]; Courtesy of Hamamatsu Phontoics]

The pixel size of the CCD chip is about 10 μm, small enough to not limit the resolution. With a streak speed of 2 ps mm^{-1}, this size would be good for a resolution of 20 fs. The slit size selected should be on the order of the pixel's size. The resolution of a streak camera mainly is limited by space charge effects of the electron beam emitted by the cathode, dispersion effects in the optics and by the quality and speed of the streak tube. A resolution of 200 fs rms is attained by a state-of-the-art camera. [11.32], [11.33]

For low charge beams, photon yield may be an issue. Even though streak cameras can detect single photons, a substantial amount of light could be lost by optical filters used to reduce dispersion effects. In addition, OTR has a low photon yield at low energies. An increased yield is obtained by Cherenkov radiators (Aerogel [11.34] or Sapphire). Synchrotron radiation is used for beam energies above 100 MeV, where the photon yield in the range of optical wavelengths is reasonable.

Figure **11.13** is an image of an electron bunch measured with a FESCA-200 [11.32]. The figure shows the time domain of the beam, where the streak direction is vertical and the horizontal direction is the transverse profile of the beam. The resolution of a streak camera is good enough for the typical bunch lengths obtained at RF guns. Streak cameras can also be used to measure the pulse length of the photoinjector laser. For compressed bunches with femtosecond scale duration, other methods need to be applied (detailed in the next sections).

Figure 11.13. Example of an image obtained by a high resolution streak camera. The streak direction is vertical. The full range of the vertical scale is 100 ps with a resolution of 1 ps. A sub-structure is visible in the time domain with a picosecond scale, which is a function of horizontal position. This demonstrates the instrument's power of detection.

11.4.2 Transverse Deflecting RF Structure

The transverse deflecting RF structure (TDS) provides a direct method to measure the shape and length of the electron bunch. [11.35]–[11.38] Figure **11.14** displays a schematic drawing of a SLAC S-band TDS. The operating principle is similar to that of a streak camera (Figure **11.15**). The RF field of the structure deflects the electron beam, either vertically or horizontally. [11.39]–[11.41] Usually, the bunch is set to the zero crossing of the field, where the time dependence of the RF field is linear and has the steepest slope.
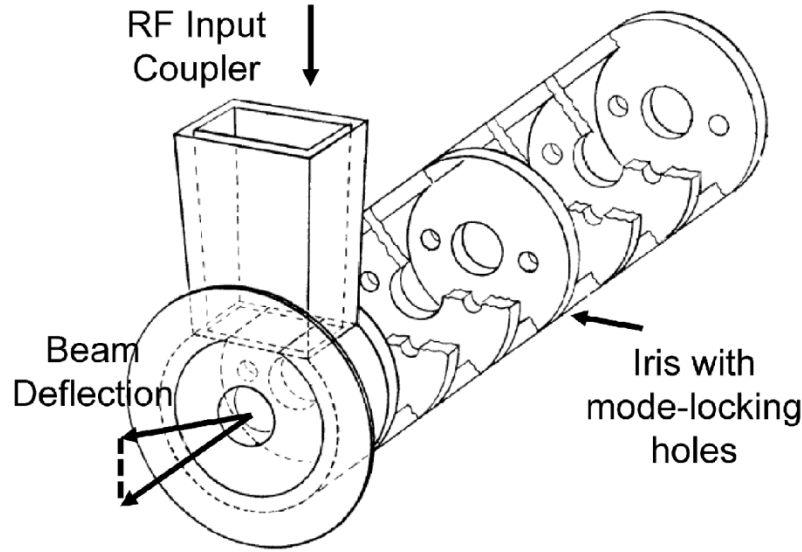

Figure 11.14. Schematic drawing of a SLAC S-band TDS. The kick is vertical in this drawing. [Reprinted with permission from [11.40]. Copyright 1964, American Institute of Physics.]
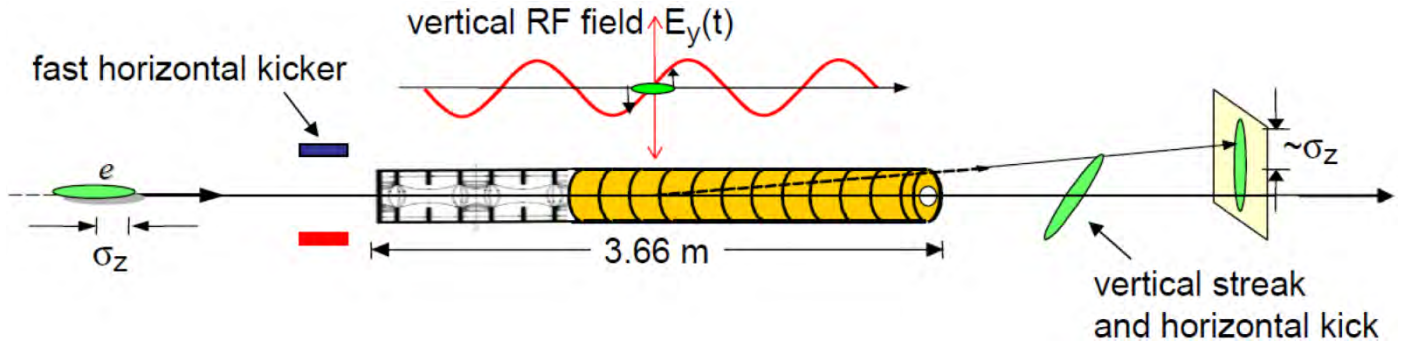

Figure 11.15. Schematic drawing of the operating principle of a transverse deflecting structure (adapted from [11.42]). The beam enters from the left and is "streaked" by the RF cavity. For bunch trains, a fast kicker may be used to pick one bunch and move it to an off-axis screen letting all other bunches safely pass the screen. [[11.42]; Courtesy of C. Behrens, DESY]

The deflection is proportional to the field, and thus, due to the time dependence of the field, is proportional to the arrival time of the electrons, or in other words, to the longitudinal position z of the electron in the bunch. As explained in [11.37], the small kick angle $\Delta x'$ as a function of longitudinal position along the bunch z is given approximately by

$$\Delta x'(z) = \frac{eV_0}{pc} \sin(kz + \phi) \approx \frac{\frac{eV_0}{p_z c}}{} \left[\frac{2\pi}{\lambda} z \cos(\phi) + \sin(\phi) \right] \tag{11.15}$$

where V_0 is the peak voltage, p is the beam momentum, λ is the RF wavelength of the structure, k is the wave number such that $k = 2\pi \lambda^{-1}$, and ϕ is the RF phase. At zero crossing, $\phi = 0$. The approximation is made that $|z| \ll \lambda/(2\pi)$, and only the linear term in z is retained.

The streaked electron bunch is imaged on a screen placed downstream of the TDS. Including the transport of the beam from the TDS to the screen with an angular to spatial element defined as

$$R_{12} = \sqrt{\beta_d \beta_s} \, \sin(\Delta \Psi) \tag{11.16}$$

the position Δx of the deflected electrons on the screen is obtained by [11.37]

$$\Delta x(z) = \frac{eV_0}{pc} R_{12} \left[\frac{2\pi}{\lambda} z\cos(\phi) + \sin(\phi) \right] \tag{11.17}$$

with the beta-functions β_d at the deflector and β_s at the screen position, and $\Delta \Psi$ is the betatron phase advance from the deflector to the screen.

From this we can calculate the rms size σ_x of the streaked beam on the screen

$$\sigma_x^2 = \sigma_{x,s}^2 + \sigma_z^2 R_{12}^2 \left[\frac{eV_0}{pc} \frac{2\pi}{\lambda} \cos(\phi) \right]^2 \tag{11.18}$$

The size of the streaked beam depends on the rms length of the bunch, σ_z, and also on the rms size of the unstreaked transverse bunch at the screen location, $\sigma_{x,s}$, i.e., the beam size when no deflecting voltage is applied. The bunch length will dominate the width of the streaked bunch if the chosen voltage is high enough, such that

$$V_0 > \frac{\lambda}{\pi \sigma_z |\cos(\phi)|} \frac{\sigma_x \gamma E_e}{R_{12}} \tag{11.19}$$

with the electron rest energy of $E_e = 511$ keV. The unit of the voltage V_0 in Equ. 11.19 is in volts if E_e is given in electron volts.

As an example, for LCLS ($p = 5$ GeV c^{-1}, $\beta \approx 50$ m, $\sigma_z = 24$ μm, $\sigma_{x,s} \approx 70$ μm), a voltage of more than 10 MV should be applied for an S-band structure ($\lambda = 10.5$ cm). [11.37]

The bunch length is calculated from Equ. 11.18 with the following expression

$$\sigma_z = \sqrt{\sigma_x^2 - \sigma_{x,s}^2} \, \frac{\lambda}{2\pi} \frac{1}{eV_0} \frac{pc}{|\sin(\Psi) \cos(\phi)|} \frac{1}{\sqrt{\beta_d \beta_s}} \tag{11.20}$$

An advantageous phase advance is near $\pi/2$ and an RF phase near zero-crossing, $\cos(\phi) = \sin(\Psi) = 1$. If the beam has a momentum chirp along the bunch, which for example is the case for beams compressed by chicane bunch compressors, a correction term has to be applied. As shown in [11.37], the effect of a linear momentum correlation along the bunch can be eliminated by choosing $\phi = 0$, or by taking the average bunch

length measured at the two phases $\phi = \phi_0$ and $\phi = \pi - \phi_0$, respectively. The rms time resolution obtained with a TDS can be as small as 10 fs.

The streaked beam can be passed through a dispersive section in the plane that is not streaked. Then, the image directly shows the longitudinal phase space: Time on one coordinate and energy on the other. Figure **11.16** is an example of the measurement of the longitudinal phase space at FLASH. A single shot measurement of the longitudinal phase space is a powerful tool to measure and tune the performance of an FEL, for example.
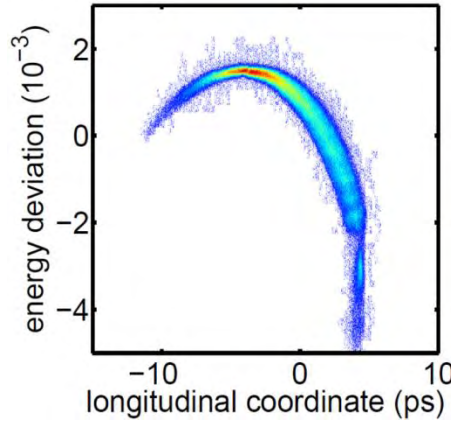

Figure 11.16. Example of a single shot image showing the longitudinal phase space distribution of a single electron bunch measured with the deflecting cavity LOLA at FLASH. The colors indicate the charge density: blue is a low density and red is a high density. [Courtesty of C. Behrens]

Burst mode machines with narrowly spaced bunches use a fast kicker system to select one bunch from the bunch train. The bunch to be analyzed is kicked on an off-axis screen, while all other bunches proceed on their usual path to the dump. In this case, the RF pulse of the TDS must be shorter than the bunch distance.

11.4.3 Frequency Domain Measurements

Frequency domain measurements use coherent radiation emitted by the electron bunch (transition, diffraction, or synchrotron radiation). A bunch emits coherently in wavelengths longer than the bunch length or the longitudinal microstructures of the bunch.

The radiation power spectrum of the coherent radiation, $P_{coh}(\omega)$, emitted by a bunch of N particles can be expressed by

$$P_{coh}(\omega) = P_s(\omega)\, N^2\, |F(\omega)|^2 \tag{11.21}$$

where $P_s(\omega)$ is the radiation power spectrum of a single particle, $F(\omega)$ is the longitudinal form factor of the bunch and ω is the frequency of the emitted radiation. $P_s(\omega)$ can be calculated analytically, and thus the measurement of the coherent radiation power spectrum directly yields $|F(\omega)|$. The longitudinal charge distribution, *i.e.*, bunch shape, is the inverse Fourier transform of the form factor.

A Martin-Puplett interferometer is an example of a device used for measuring longitudinal bunch shape. [11.43], [11.44]

It is based on the measurement of the autocorrelation function of the incoming radiation pulse in the terahertz wavelength range. Electron bunches with a length in the 50 μm to millimeter scale radiate coherently in the terahertz spectral range. As a radiator, diffraction radiation from off-axis screens or from a slit screen is often used. The coherent radiation pulse is guided out of the electron beam pipe through a suitable window. Diamond is the best choice, and single crystal quartz is also used. It is important that the window is transparent to the wavelength of interest and the beam path is evacuated to avoid frequency dependent absorption of the radiation, for example, by water. Wire grids are used to polarize and split the pulse into two beams. A beam splitter, which transmits one polarization and reflects the other, is used to divide and recombine the two pulses after flipping their polarization by roof mirrors. The recombined radiation is elliptically polarized; the degree of polarization depends on the path difference between the two arms. By varying the path length of one arm, the autocorrelation function is measured. The horizontal- and vertical-polarization components are measured by two broadband detectors, such as pyroelectric detectors or Golay cells. A Fourier transform of the autocorrelation function gives the magnitude of the form factor. However, this method does not include phase information, which is also required to determine the longitudinal charge distribution. The phase must be calculated analytically, for example by using a Kramers-Kronig relation. [11.45] In practice, the data analysis for this method is quite complicated and several frequency dependent corrections need to be considered.

11.4.4 Electro-Optical Sampling Method

Electro-optical (E-O) sampling is a technique to measure the shape and length of short bunches. It is based on detecting the electric field of the electron bunch as it passes closely to a non-linear optical crystal, for example, ZnTe. The electric field inside the crystal is influenced by the electron bunch and can be probed by an initially linearly polarized femtosecond laser pulse. The laser pulse becomes elliptically polarized and the measurement of its polarization yields information on the longitudinal distribution of the electron bunch. Electro-optical sampling methods are detailed in [11.42]. Figure **11.17** is an example of a set-up for temporally encoded electro-optic detection.

Using a Ti:Sa probe laser pulse of 30 fs (FWHM) duration (energy of > 100 μJ) and a 300 μm thick β-barium borate (BBO) crystal, a resolution of better than 100 fs can be reached. [11.42] Temporally resolved, electro-optic detection was first demonstrated at FELIX. [11.46]
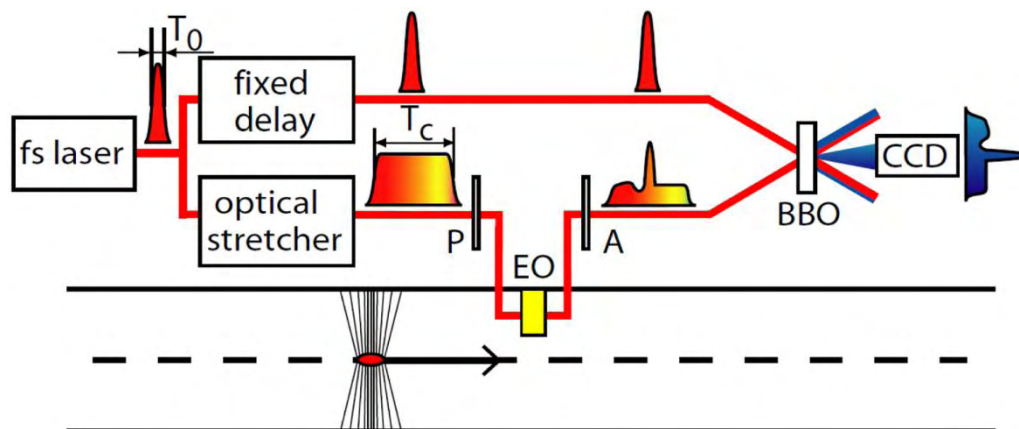

Figure 11.17. Schematic of a temporally encoded electro-optic detection set-up. The short laser pulse with a length of T_0 is split into two parts: One part is stretched to several picoseconds (T_C) and sent through the polarizer (P) and the E-O crystal (EO) in parallel with the Coulomb field of the electron bunch, while the second part remains unstretched. In the E-O crystal, the stretched laser pulse acquires an elliptic polarization with an ellipticity proportional to the electric field of the electron bunch, and with the same temporal structure. The analyzer (A) turns the elliptical polarization into an intensity modulation, which is then sampled by the short pulse in a single-shot cross-correlator. [Adapted from [11.47], with permission from Elsevier]

11.5 BEAM POSITION

Beam position monitors (BPMs) are used to measure the transverse beam position in the beamline. BPMs are usually placed along the entire beamline at appropriate locations to determine the orbit, to understand the optics response, to determine the beam energy in spectrometers and to evaluate beam jitter. In linacs, a good single shot resolution is desirable to be able to observe shot-to-shot effects. For accelerators operating in burst modes, individual bunches in a train should be resolved clearly.

There are several different types of BPMs: The basic types are broadband pickups and resonant cavity monitors. In a broadband pickup, the beam induces a signal on four electrodes which are arranged symmetrically around the beam pipe. Examples of this kind of monitor are button- and stripline-BPMs. In resonant cavity monitors, a dipole mode is excited in a cylindrical cavity by an off-axis beam. For both types of monitors, the signal depends on the transverse beam position and the bunch charge. Therefore, four symmetrically arranged electrodes (for button- and stripline-monitors) or slots (for cavity monitors) are needed to achieve a linear, charge independent measurement of the beam position. Reentrant cavity monitors are special type of cavity monitors, which are operated below the resonant frequency with a large bandwidth.

The typical single shot resolution of button monitors is ~50 μm rms, *viz.*, sufficient for most applications, especially for injectors where the beam size is still large. In general, the resolution should be less than 10% of the expected beam size. This is because most applications require a beam position jitter of less than 10% of the beam size – to be resolved by the BPMs. Examples of a very demanding requirement are undulators for FELs. Here, the single shot resolution should be in the 1 μm range. This is achieved with cavity type monitors.

The signals from the pick-ups are amplified. The signal's amplitude or its arrival time is measured with suitable sample-and-hold detectors together with good resolution ADCs. One method to determine the beam position is to measure the difference between two signals from two opposite pick-ups, normalized by their sum. For example, the horizontal beam position x is determined by

$$x = k\,\frac{h_l - h_r}{h_l + h_r} \tag{11.22}$$

where h_l and h_r are the signal amplitudes of pick-ups mounted left and right of the vacuum chamber. For instance, the calibration constant k is determined by measuring the known response of corrector magnets on the beam position. The absolute zero position (center of the vacuum chamber) is determined by carefully equalizing the amplifier gain of both arms.

11.6 ENERGY AND ENERGY SPREAD

A dispersive section of the electron beamline is used to determine the energy (or momentum) and energy spread of the beam. Such a section consists typically of a deflecting dipole magnet with a known homogeneous field and a screen located in the dispersive section. Often, beam position monitors are included.

The momentum, p, of an electron is given by

$$p = eBr \tag{11.23}$$

with the electron charge e, the magnetic field B, and the radius of the track inside the magnet, r. The beam energy, E, is obtained *via* the usual relation $E^2 = p^2c^2 + m_e^2c^4$. In practical units, Equ. 11.23 can be written as

$$p\left[\frac{\text{GeV}}{\text{c}}\right] = 0.3\ B\ [\text{T}]\ r\ [\text{m}] \tag{11.24}$$

For accurate energy measurements, the beam must be placed on the nominal pass through the dipole magnet where the field and the radius of curvature are known. A set of BPMs is used to determine the orbit through the dipole field. The dipole current is adjusted such that the beam is centered in the beamline downstream, the dispersive arm. Centering is assured using BPMs or calibrated screens. The beam momentum is then given by Equ. 11.23. Hysteresis effects have to be taken into account. A careful measurement of the field as a function of the current is mandatory.

Beam centering is not required if its position is measured accurately upstream and downstream of the dipole, and these positions must be considered when determining the relation between the beam energy and the dipole current.
The energies of the individual electrons in the bunch differ somewhat from each other. Electrons with different energies follow different paths through the dipole, and therefore end up at different locations on the downstream screen.

The momentum, p, of an electron at position x_D, with respect to the nominal center position occupied by an electron with momentum p_0, is

$$p = p_0\left(1 + \frac{x_D}{D}\right) \tag{11.25}$$

The quantity D is called the dispersion and has the dimension of length. Thus, with a dispersion of 10 mm and a screen- or position-resolution of 10 μm, a momentum resolution of 10^{-3} is obtained.

The energy spread can be determined from the transverse beam spot size. If the dipole deflects in the horizontal plane, the horizontal dimension gives the energy spread. The transverse size of the bunch needs to be taken into account. The spot width caused by the energy spread should be significantly larger than the beam's natural size. Therefore, for accurately measuring energy spread, the beam should be well focused using quadrupoles or a solenoid magnet upstream of the dipole.

A screen in a dispersive section is also often used to determine the on-crest phase of an accelerating module. With the phase on crest, energy is maximized and the correlated energy spread minimized. For adjusting the right compression for FELs, determining the on-crest phase within a degree of RF-phase is mandatory.

The correlated energy spread is induced by the sinusoidal shape of the RF field. The uncorrelated energy spread is an intrinsic property of the electron source, for example, RF gun-based sources have a very small energy spread of a few kiloelectron volts. Its smallness may induce unwanted collective effects during bunch compression due to space charge or coherent synchrotron radiation; these need to be mitigated by the so-called laser heaters, for example. [11.48]

11.7 EMITTANCE

Beam emittance characterizes the beam dynamics and is an important measure of its quality.

The emittance of an electron bunch, ε, usually is defined in terms of measurable quantities that are also applicable in simulation codes [11.49]

$$\varepsilon = \frac{1}{\overline{p}_z} \sqrt{\langle x^2 \rangle \langle p_x^2 \rangle - \langle xp_x \rangle^2} \qquad (11.26)$$

with x being the Cartesian transverse horizontal coordinate of the electron and p_x the momentum component in horizontal direction. An equivalent equation holds for the vertical component, y. For simplicity, whenever the notation x is used, the expression holds for both Cartesian coordinates. The brackets $\langle\ \rangle$ define the second central moment of the distributions, or in other words, the mean square value. For a definition, see [11.49]. Note that $\overline{p}_z$ is the average longitudinal momentum of the electrons. The coordinate z is in direction of acceleration. The emittance defined in this way is an rms emittance.
In experiments, the terms with transverse momenta p_x are often estimated by the measured beam divergence, such as

$$\sigma_x' = \left\langle \sqrt{\frac{p_x}{p_z}} \right\rangle^2 = \langle \sqrt{x'} \rangle^2 \qquad (11.27)$$

the rms beam size is

$$\sigma_x = \sqrt{\langle x^2 \rangle} \qquad (11.28)$$

Using the beam divergence, we write the rms emittance in the following form, often called trace space[2] emittance

$$\varepsilon_{\mathrm{rms}} = \sqrt{\langle x^2 \rangle \langle x'^2 \rangle - \langle xx' \rangle^2} \qquad (11.29)$$

Equ. 11.26 shows that the emittance is adiabatically damped with the average longitudinal beam momentum, $\overline{p}_z$. Therefore, it is convenient to define a normalized emittance, ε_n, to be

$$\varepsilon_n = \frac{\overline{p}_z}{m_e c} \varepsilon_{geo} \approx \gamma \varepsilon_{geo} \qquad (11.30)$$

where ε_{geo} is sometimes called the geometrical emittance. Here, γ is the relativistic factor as defined in Equ. 11.12. Although the geometrical emittance decreases as a function of increasing beam energy, the normalized emittance stays constant. Therefore, normalized emittance commonly is used to characterize the beam.
The emittance, as defined above, is equivalent to the Courant-Snyder invariant, $W = \varepsilon$, which is given by [11.50]

---

[2]Usually, we talk about *phase space* when we use the space coordinates x together with the momentum p_x of the particles; *trace space* is used to express, that the angular coordinate x' is used rather than p_x.

$$W = \gamma x^2 + 2\alpha xx' + \beta x'^2 \tag{11.31}$$

α, β and γ are the Twiss-parameters, and $x' = dx/dz$; z is the direction of motion. These parameters should not be confused with the relativistic β and γ parameters. The relation between emittance and beam size in terms of the Courant-Snyder beta-function, $\beta(z)$, is

$$\sigma_x^2(z) = \varepsilon\beta_x(z) \tag{11.32}$$

As an example, a beam size of $\sigma_x = 100$ μm with a beta-function $\beta_x(z)$ of 10 m is achieved with an emittance of $\varepsilon = 1$ nm.

To determine the emittance, the second central moments $\langle x^2 \rangle$, $\langle x'^2 \rangle$ and $\langle xx' \rangle$ must be measured. This can be done by different methods: A slit mask, a quadrupole scan, or a multi-monitor method.

A typical emittance of a 1 nC electron bunch produced by a photoinjector RF gun is between 1-2 mm mrad. Often the emittance is expressed in micrometers, omitting the angular unit.

A detailed description of how to measure emittance, including a brief theoretical background and a discussion on systematic measurement errors, is given in [11.51].

11.7.1 Slit Mask Technique

The slit technique typically is used at low beam energies, where the space charge effects of the drifting beam would not allow a measurement of the true beam divergence. If we neglect space charge effects, a drifting beam along z from $z = 0$ to $z = L$ would change its transverse size, $\sigma_x(z)$, according to its emittance by

$$\sigma_x(L) = \sigma_x(0) + \sigma_x' L \tag{11.33}$$

A beam with this behavior is called an *emittance* dominated beam. σ_x' is the beam divergence as defined in Equ. 11.27.

In a space charge dominated beam, we can cut out small portions of the beam such that the resulting beamlets are now emittance dominated. After a certain drift, the beamlets are imaged with an OTR or fluorescence screen, where their size is measured.

To do this, a mask with one or several slits cuts the beam into these beamlets. The size of the slits is small enough so that the effect of space charge can be neglected. As an example, for a typical beam with a charge of 1 nC, a beam size of 1 mm, a nominal emittance of 1-10 μm, and a slit width of 50 μm are usually taken. The thickness of the mask is large enough to provide a good stopping power of the electrons cut. A stainless steel mask for a beam with a few megaelectron volts typically is 5 mm thick. The separation between the slits is larger than the slit's width (1 mm) in order to keep the beamlets well separated after the drift. The drift distance to the screen is about 50 cm. The values above are an example taken from [11.52]. A mask with several slits is difficult to manufacture, but has the advantage of a simultaneous measurement of the whole beam. In contrast, the single slit needs to be scanned through the beam.

A detailed description of the slit mask technique is given in [11.52], [11.53], where space charge effects are also discussed.

Figure **11.18** shows a schematic layout of a multi-slit-based emittance measurement. The space charge dominated beam passes through a mask with multiple slits yielding emittance dominated beamlets.

The parameters needed to determine the emittance as defined in Equ. 11.29 are derived from the beam image: the overall envelope formed by the beamlets gives $\langle x \rangle^2$, the distance between the beamlet centroids is proportional to $\langle xx' \rangle$ and the width of the beamlets gives $\langle x'^2 \rangle$. There are several techniques for calculating these parameters from the measured slit images. [11.53], [11.54]

Instead of using slits, a mask consisting of many small holes, the so-called "pepper-pot," is used for single shot, 2-D emittance measurements. [11.55]
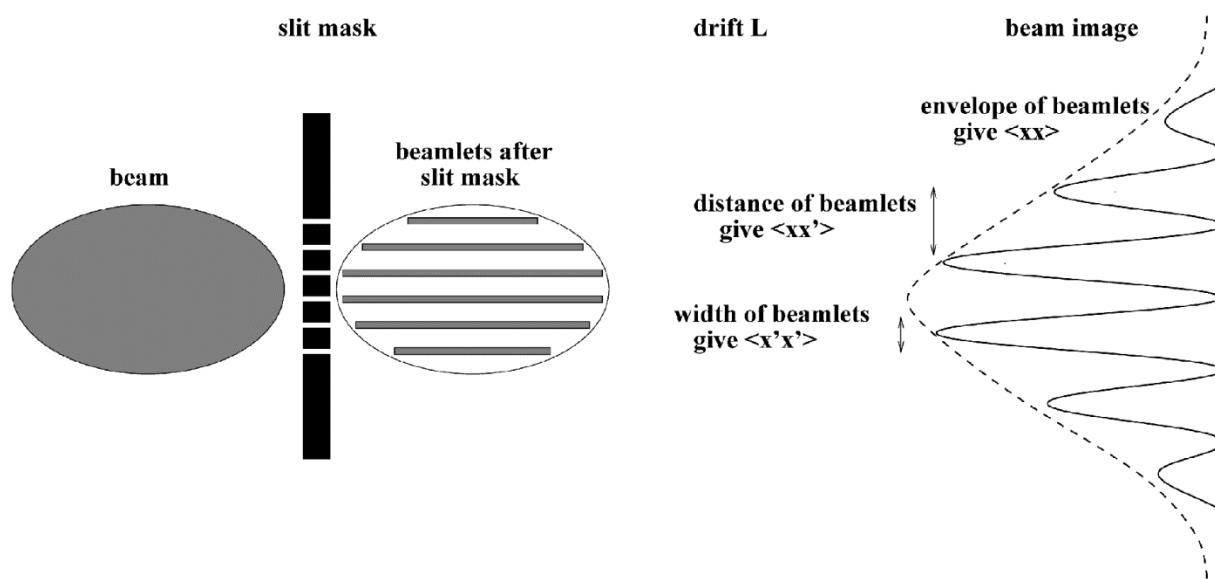

Figure 11.18. Schematic scheme of an emittance measurement based on multi-slits. The beam is cut into small beamlets which drift the distance L to the observation screen. [Courtesy of K. Honkavaara, DESY]

Slits are used at the exit of RF guns, for high beam energies after considerable acceleration, to say 100 MeV or more; thereafter, slits become inappropriate and other methods are more convenient. They are discussed in the next sections.

11.7.2 Quadrupole Scan Method

In the quadrupole scan method, the beam size is measured for different settings of one or more quadrupole magnets placed upstream of the beam size monitor (a screen or a wirescanner). The beam optics (transfer matrices) for different quadrupole settings is calculated and a parabolic fit of the beam sizes measured for the different settings gives the needed beam parameters to determine the emittance. The principle of this method is equivalent to measuring M^2 for laser beams, where M^2 is the ratio of the beam parameter product, waist size times divergence, of the given laser beam to that of an ideal Gaussian beam. The "focusability" of the beam is a measure of its emittance.

The disadvantage of this method is that the beam optics must be changed for each measurement point and thus it is not suitable if beam losses induced by the scan cannot be transported safely to the dump.
In injectors, the beam power usually is small so that the beam can be dumped somewhere in the beam pipe. Another issue is that very small spot sizes may be obtained at the focal point of the quadrupole. The space charge density at the focus can be so large that its effect is not negligible and needs to be considered.

There may be a problem with resolution; small beam sizes, say less than 50 μm, are difficult to measure with standard methods. On the other hand, good resolution comes with a small field view, which precludes measuring larger spot sizes. To gain a good dynamic range, several magnifications of the optical viewing system are required.

Let us use matrix formalism to describe the beam optics. The transverse trace space of the beam is described by the beam matrix M, which is a function of the direction of motion z (as an example, refer to [11.51], [11.56])[3]

$$M(z) = \begin{pmatrix} M_{11} & M_{12} \\ M_{21} & M_{22} \end{pmatrix}$$

(11.34)

The matrix elements are defined as the second moments of the transverse coordinate x, also expressed in terms of the Twiss-parameters and the emittance

$$M_{11} = \langle xx \rangle = \beta\varepsilon \; ; M_{12} = M_{21} = \langle xx' \rangle = -\alpha\varepsilon \; ; M_{22} = \langle x'x' \rangle = \gamma\varepsilon$$

(11.35)

The motion of the beam, from a position z_0 to a position z further downstream along the beamline, can be described by a transfer matrix R. The beam matrix at position z is then calculated by

$$M(z) = R \, M(z_0) \, R^{\mathrm{T}}$$

(11.36)

The emittance can now be determined by measuring the transverse beam size at a location z as a function of the current of a quadrupole magnet. The transfer matrix then becomes a function of the current or the magnet field gradient, g, of the quadrupole. The square of the beam size $\langle x^2 \rangle = M_{11}$ is given by

$$M_{11}(z) = M_{11}(z_0) \, R_{11}(g)^2 + 2M_{12}(z_0) \, R_{11}(g) \, R_{12}(g) + M_{22}(z_0) \, R_{12}(g)^2$$

(11.37)

The transport matrix includes drifts and the quadrupole. Figure **11.19** shows a simulated quadrupole scan.

With a fit to the measured data, the relevant matrix elements are evaluated to determine the emittance according to Equ. 11.29, using Equ. 11.37 and Equ. 11.35.

To overcome potential systematic errors due to space charge effects, using two or more quadrupoles will keep the beam spot size large enough. Furthermore, this method has the advantage that the beam size can be kept sufficiently small so that the entire beam fits on to the screen.

In the next section, I describe the multi-monitor method that avoids the space charge effect and does not require a change of the beam optics.

---

[3]Often, the Greek letter σ is used for the beam matrix. We use M to avoid confusion with the beam size σ.
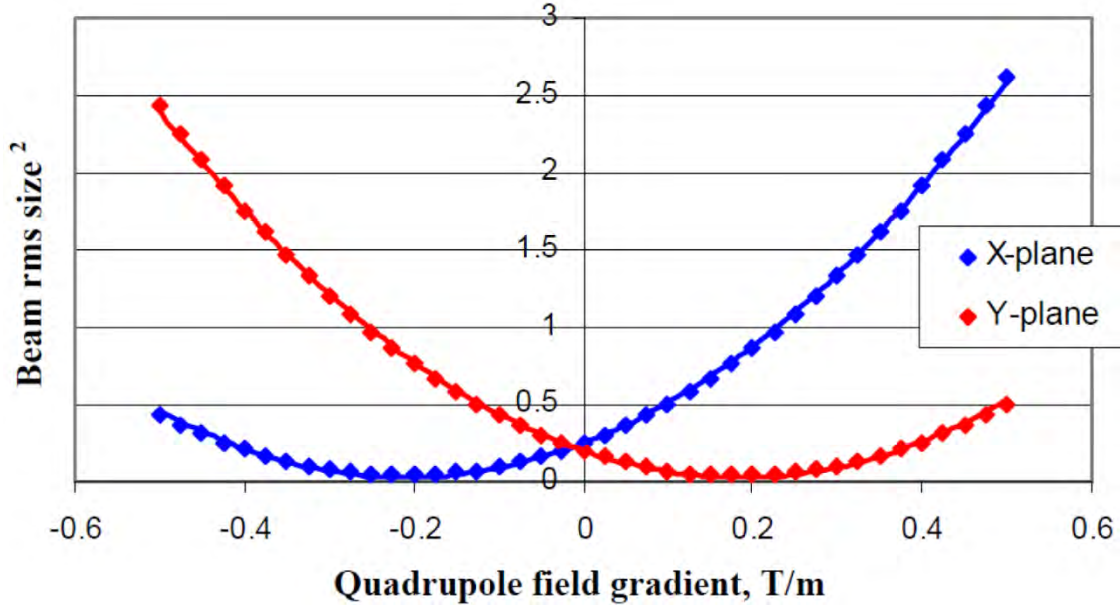
Figure 11.19. Simulated quadrupole scan. The quadrupole gradient is plotted as a function of the squared-beam size at a certain position *z* downstream from the quadrupole. In this example, the focal point for the horizontal- and vertical-coordinate appears at different gradients. The beam size is given in millimeters. [[11.56]; Courtesy of S. Skelton]

11.7.3 Multi-Monitor Method

In a multi-monitor method, the beam size is measured at three or more locations without changing the beam optics [11.57]. A typical set-up consists of a period FODO magnet lattice of focusing- and defocusing-quadrupoles, together with four screens or wirescanners. A FODO lattice is a periodic structure. One period consists of a focusing element (F), usually a quadrupole, a drift (O), a defocusing element (D) and an additional drift (O).

The parameters required for assessing emittance are determined from the measured sizes of the beam by fitting the transport function or by using tomographic phase space reconstruction methods. The advantage of the multi-monitor method is that the beam optics is fixed and the beam size on the screens can be chosen such that a good resolution is obtained. Fixed beam optics avoid a scan of the magnetic field of quadrupoles. Hysteresis effects of the quadrupole magnets, beam losses during scans are avoided and set-up time is reduced. However, a set-up with a FODO lattice, including a matching section, requires considerable space for beamline elements; several quadrupoles and screen stations have to be realized. The matching section is useful to adapt the optics to be optimal for the emittance measurement. Once such a section is established in an accelerator, it can also serve to match the optics emerging from the injector to the accelerator. The measurement yields all Twiss-parameters from Equ. 11.31 (α, β, γ) required to match to the optics of the accelerator.

As an example, Figure **11.20** shows the matching and FODO section in the FLASH injector that is 10 m long, with 12 quadrupoles and 4 OTR/wirescanner stations.

Loehl *et al.* give a detailed description of emittance measurements at FLASH using the multi-monitor method [11.14], [11.51].

Figure 11.20. Picture of the diagnostic section of the FLASH injector. Four screen stations equipped with wire scanners in a FODO lattice with several quadrupole magnets are employed in measuring Twiss-parameters of the beam.

Using Equ. 11.36 and Equ. 11.35, we can write a similar expression as for the quadrupole scan method (Equ. 11.37)

$$M_{11}(z_i) = M_{11}(z_0) R_{11}(z_i)^2 + 2M_{12}(z_0) R_{11}(z_i) R_{12}(z_i) + M_{22}(z_0) R_{12}(z_i)^2 \tag{11.38}$$

Here, the matrix elements are evaluated at a position $z = z_i$. When we now measure the squared-beam size $\langle x_i^2 \rangle = M_{11}(z_i)$ at three different locations z_i, where $i = 1, 2, 3$, we obtain the three relevant beam matrix elements from

$$\begin{pmatrix} \langle x_0^2 \rangle \\ \langle x_0 x_0' \rangle \\ \langle x_0'^2 \rangle \end{pmatrix} = \mathfrak{R}^{-1} \begin{pmatrix} \langle x_1^2 \rangle \\ \langle x_2^2 \rangle \\ \langle x_3^2 \rangle \end{pmatrix} \tag{11.39}$$

with the matrix $\mathfrak{R}$ given by

$$\mathfrak{R} = \begin{pmatrix} R_{11}^2(z_1) & R_{11}(z_1)R_{12}(z_1) & R_{12}^2(z_1) \\ R_{11}^2(z_2) & R_{11}(z_2)R_{12}(z_2) & R_{12}^2(z_2) \\ R_{11}^2(z_3) & R_{11}(z_3)R_{12}(z_3) & R_{12}^2(z_3) \end{pmatrix} \tag{11.40}$$

The emittance is then calculated with Equ. 11.29 where the Twiss parameters at $z = z_0$ are determined by Equ. 11.35.

The information about the beam lattice is contained in the matrix $\mathfrak{R}$ and needs to be known accurately. A discussion of the systematic errors involved appears in [11.51].

Correctly choosing the phase advance between the screens is a key in optimizing the system's resolution power. A phase advance of 180° between screens would mean that the same information is always measured. The optimal phase advance would be one wherein screens are equally placed in the 180° phase

advance space, taking into account that 0° and 180° measure the same beam. Therefore, we obtain 60° for three screens, 45° for four screens, and so on.

In the discussion above, I assumed a vanishing dispersion. In the presence of a non-zero dispersion, this method can be extended to encompass the dispersion function and the angular dispersion function. Here, at least six measurements of the beam size at appropriate places are needed.

It is also possible to measure the coupling between the horizontal and the vertical plane; at least four measurements are required for this.

Even though three measurements would suffice to give the Twiss parameters, more screens allow using fitting methods, thereby increasing the measurement's precision.

11.7.4 Tomographic Reconstruction of the Phase Space

The phase space description with Twiss parameters assumes a homogeneous distribution of the electrons in the phase space. Since this is often not the case, tomographic methods generate more information about the distribution of electrons in the phase space. These methods also access information about possible tails in the distribution. With the pure statistical approach using an emittance defined by the second-order moments of the distribution, tails have a large weight, and thus greatly influence the rms emittance.

The tomographic reconstruction uses measurements of the phase space from different projections. Many methods require a large number of projections, which is difficult to realize experimentally. [11.58] The maximum entropy algorithm (MENT) provides a reconstruction from a few projections only. A comprehensive description of the MENT algorithm is given in [11.59]–[11.62].

Temporally resolved slice emittance measurements using the quadrupole scan technique together with a transverse deflecting cavity is a good method of reconstructing the transverse phase space as a function of longitudinal position within the electron bunch using tomographic methods as detailed in [11.63] and [11.64].

11.8 CONFLICT OF INTEREST AND ACKNOWLEDGEMENT

References
[11.1] P. Strehl, *Beam Instrumentation and Diagnostics*, Berlin: Springer, 2005.
[11.2] D. Lipka, W. Kleen, J. Lund-Nielsen *et al.*, "Dark current monitor for the European XFEL," in *Proc. 10th European Workshop Beam Diagnostics Instrumentation Particle Accelerators*, 2011, May 2011.
[11.3] K. L. Brown and G. W. Tautfest, "Faraday-cup monitors for high-energy electron beams," *Rev. Sci. Instrum.*, vol. 27, pp. 696-702, September 1956.
[11.4] L. Bess and A. O. Hanson, "Measurement of the electron current in a 22-mev betatron," *Rev. Sci. Instrum.*, vol. 19, pp. 108-110, February 1948.
[11.5] L. Bess, J. Ovadia and J. Valassis, "External beam current monitor for linear accelerators," *Rev. Sci. Instrum.*, vol. 30, pp. 985-988, November 1959.
[11.6] R. Yamada, "New magnetic pickup probe for charged particle beams," *Japanese J. Appl. Phys.*, vol. 1, pp. 92-100, 1962.

[11.7] S. N. Gardiner, J. L. Matthews and R. O. Owens, "An accurate non-intercepting beam current integrator for pulsed accelerator beams," *Nucl. Instrum. Meth.*, vol. 87, pp. 285-290, October 1970.

[11.8] K. B. Unser, "Design and preliminary tests of a beam intensity monitor for LEP," in *Proc. 1989 Particle Accelerator Conf.*, 1989, pp. 71-73.

[11.9] J. Bergoz, "Current monitors for particle beams," *Nucl. Physics A*, vol. 525, pp. 595-600, April 1991.

[11.10] Vacuumschmelze GmbH & Co. KG, Gruener Weg 37, 63450 Hanau, Germany, http://www.vacuumschmelze.de/.

[11.11] P. Forck, "Lecture notes on beam instrumentation and diagnostics," Archamps: Joint University Accelerator School, January 3-March 11 2011, http://www-bd.gsi.de/conf/juas/juas_script.pdf.

[11.12] L. Wartski, S. Roland, J. Lasalle *et al.*, "Interference phenomenon in optical transition radiation and its application to particle beam diagnostics and multiple-scattering measurements," *J. Appl. Phys.*, vol. 46, 3644-3653, August 1975.

[11.13] L. Wartski, "Study of optical transition radiation produced by 30 to 70 MeV energy electrons: Applications to the diagnostics of beams with charged particles," Ph.D. Thesis, Paris-Sud University, Orsay, France, 1976.

[11.14] F. Löhl, S. Schreiber, M. Castellano *et al.*, "Measurements of the transverse emittance at the FLASH injector at DESY," *Phys. Rev. ST Accel. Beams*, vol. 9, pp. 092802-1–092802-6, September 2006.

[11.15] Basler AG, An der Strusbek 60-62, 22926 Ahrensburg, Germany, http://www.baslerweb.com/index.html.

[11.16] R. W. Allison Jr., R. W. Brokloff, R. L. McLaughlin *et al.*, "A radiation-resistant chromium-activated aluminum oxide scintillator," Lawrence Berkley Radiation Laboratory, Technical Report No. UCRL-19270, July 1969.

[11.17] C. D. Johnson, "The development and use of alumina ceramic fluorescent screens," European Laboratory for Particle Physics, Technical Report No. CERN/PS/90-42(AR), October 1990.

[11.18] MAC-A994R, available by Morgan Technical Ceramics, 55-57 High Street, Windsor, Berkshire, U.K., SL4 1LP. Available at http://www.morgantechnicalceramics.com/download.php?5151434153695931675250727139694b714e33346d696d4675694a784e6150714d6c54785842453058532f2b.

[11.19] W. S. Graves, E. D. Johnson and P. G. O'Shea, "A high resolution electron beam profile monitor," in *Proc. 1997 Particle Accelerator Conf.*, 1997, pp. 1993-1995.

[11.20] A. Murokh, J. Rosenzweig, V. Yakimenko *et al.*, "Limitations on the resolution of YAG:Ce beam profile monitor for high brightness electron beam," in *Proc. 2ⁿᵈ Int. Committee Future Accelerators Advanced Accelerator Workshop Physics High Brightness Beams*, 2000, pp. 564-580.

[11.21] Saint-Gobain Crystals, 18900 Great Lakes PKWY, Hiram, OH 44234-9681, USA, "YAG(Ce) Yttrium Aluminum Garnet Scintillation Material," http://www.detectors.saint-gobain.com/uploadedFiles/SGdetectors/Documents/Product_Data_Sheets/YAG-Data-Sheet.pdf.

[11.22] X. Artru, R. Chehab, K. Honkavaara *et al.*, "Resolution power of optical transition radiation: Theoretical considerations," *Nucl. Instrum. Meth. B*, vol. 145, pp. 160-168, October 1998.

[11.23] K. Honkavaara, Optical Transition Radiation in High Energy Electron Beam Diagnostics, Helsinki: Helsinki Institute of Physics, 1999.

[11.24] R. Jung and R. J. Colchester, "Development of beam profile and fast position monitors for the LEP injector linacs," *IEEE Trans. Nucl. Sci.*, vol. 32, pp. 1917-1919, October 1985.

[11.25] R. Fulton, J. Haggerty, R. Jared *et al.*, "A high resolution wire scanner for micron-size profile measurements at the SLC," *Nucl. Instrum. Meth. A*, vol. 274, pp. 37-44, January 1989.

[11.26] M. C. Ross, "Wire scanner systems for beam size and emittance measurements at SLC," in *AIP Conf. Proc.*, vol. 229, 1991, pp. 88-106.

[11.27] U. Hahn, N. V. Bargen, P. Castro *et al.*, "Wire scanner system for FLASH at DESY," *Nucl. Instrum. Meth. A*, vol. 592, pp. 189-196, July 2008.

[11.28] J. Camas, C. Fischer, J. J. Gras *et al.*, "Observation of thermal effects on the LEP wire scanners," in *Proc. 1995 Particle Accelerator Conf.*, vol. 95, 1995, pp. 2649-2651.

[11.29] C. Yan, P. Adderley, D. Barker *et al.*, "Superharp – a wire scanner with absolute position readout for beam energy measurement at CEBAF," *Nucl. Instrum. Meth. A*, vol. 365, pp. 261-267, November 1995.

[11.30] Ch. Gerth, J. Feldhaus, K. Honkavaara *et al.*, "Bunch length and phase stability measurements at the TESLA test facility," *Nucl. Instrum. Meth. A*, vol. 507, pp. 335-339, July 2003.

[11.31] M. Uesaka, T. Ueda, T. Kozawa *et al.*, "Precise measurement of a subpicosecond electron single bunch by the femtosecond streak camera," *Nucl. Instrum. Meth. A*, vol. 406, pp. 371-379, April 1998.

[11.32] Femtosecond streak camera C6138 (FESCA-200), available by Hamamatsu Photonics K.K., Hamamatsu, Japan. Available at http://jp.hamamatsu.com/resources/products/sys/pdf/eng/e_c6138.pdf.

[11.33] T. Watanabe, M. Uesaka, J. Sugahara *et al.*, "Subpicosecond electron single-beam diagnostics by a coherent transition radiation interferometer and a streak camera," *Nucl. Instrum. Meth. A*, vol. 437, pp. 1-11, November 1999.

[11.34] J. Roensch, J. Rossbach, G. Asova *et al.*, "Investigations of the longitudinal beam properties at the photoinjector test facility in Zeuthen," in. *Proc. 2006 Free Electron Laser Conf.*, 2006, pp. 597-600.

[11.35] R. H. Miller, R. F. Koontz and D. D. Tsang, "The SLAC injector," *IEEE Trans. Nucl. Sci.*, vol. 12, pp. 804-808, June 1965.

[11.36] X.-J. Wang, "Producing and measuring small electron bunches," in *Proc. 1999 Particle Accelerator Conf.*, 1999, pp. 229-233.

[11.37] P. Emma, J. Frisch and P. Krejcik, "A Transverse RF deflecting structure for bunch length and phase space diagnostics," Stanford Linear Accelerator Laboratory, Technical Report No. LCLS-TN-00-12, August 2000.

[11.38] R. Akre, L. Bentson, P. Emma *et al.*, "A transverse RF deflecting structure for bunch length and phase space diagnostics," Stanford Linear Accelerator Center, Technical Report SLAC-PUB-8864, June 2001.

[11.39] O. H. Altenmueller, R. R. Larsen and G. A. Loew, "Investigations of traveling wave separators for the Stanford two-mile linear accelerator," Stanford Linear Accelerator Center, Technical Report No. SLAC-R-0017, August 1963.

[11.40] O. H. Altenmueller, R. R. Larsen and G. A. Loew, "Investigation of traveling wave separators for the Stanford two-mile linear accelerator," *Rev. Sci. Instrum.*, vol. 35, pp. 438-442, April 1964.

[11.41] G. A. Loew and O. H. Altenmueller, "Design and applications of RF separator structures at SLAC," Stanford Linear Accelerator Center, Technical Report No. SLAC-PUB-0135, August 1965.

[11.42] B. Steffen, "Electro-optic methods for longitudinal bunch diagnostics at FLASH," Ph.D. Thesis, Universität Hamburg, Hamburg, Germany, 2007.

[11.43] L. Frölich and O. Grimm, "Bunch length measurements using a Martin-Puplett interferometer at the VUV-FEL," Ph.D. Thesis, Universität Hamburg, Hamburg, Germany, 2005.

[11.44] R. Lai and A. J. Sievers, "On using the coherent far IR radiation produced by a charged-particle bunch to determine its shape: I Analysis," *Nucl. Instrum. Meth. A*, vol. 397, pp. 221-231, October 1997.

[11.45] R. Lai and A. J. Sievers, "Determination of a charged-particle-bunch shape from the coherent far infrared spectrum," *Phys. Rev. E*, vol. 50, pp. R3342-3344, November 1994.

[11.46] G. Berden, S. P. Jamison, A. M. MacLeod *et al.*, "Electro-optic technique with improved time resolution for real-time, nondestructive, single-shot measurements of femtosecond electron bunch profiles," *Phys. Rev. Lett.*, vol. 93 , 114802-1–114802-4, September 2004.

[11.47] S. P. Jamison, G. Berden, A. M. MacLeod *et al.*, "Electro-optic techniques for temporal profile characterisation of relativistic coulomb fields and coherent synchrotron radiation," *Nucl. Instrum. Meth A*, vol. 557, pp. 305-308, February 2006.

[11.48] E. L. Saldin, E. A. Schneidmiller and M. V. Yurkov, "Longitudinal space charge-driven microbunching instability in the TESLA Test Facility linac," *Nucl. Instrum. Meth. A*, vol. 528, pp. 355-359, August 2004.

[11.49] K. Floettmann, "Some basic features of the beam emittance," *Phys. Rev. ST Accel. Beams*, vol. 6, pp 034202-1–034202-7, March 2003.

[11.50] E. D. Courant and H. S. Snyder, "Theory of the alternating-gradient synchrotron," *Ann. Physics*, vol. 3, pp. 1-48, January 1958.

[11.51] F. Löhl, "Measurements of the transverse emittance at the VUV-FEL," Ph.D. Thesis, Universität Hamburg, Hamburg, Germany, 2005.

[11.52] S. G. Anderson, J. B. Rosenzweig, G. P. LeSage *et al.*, "Space-charge effects in high brightness electron beam emittance measurements," *Phys. Rev. ST Accel. Beams*, vol. 5, 014201-1–014201-12, January 2002.

[11.53] S. G. Anderson, "Creation, manipulation, and diagnosis of intense, relativistic picosecond photo-electron beams," Ph.D. Thesis, University of California Las Angeles, Las Angeles, Californaia, 2002.

[11.54] L. Staykov, "Characterization of the transverse phase space at the photo-injector test facility in DESY, Zeuthen site," Ph.D. Thesis, Universität Hamburg, Hamburg, Germany, 2008.

[11.55] S. C. Hartmann, N. Barov, C. Pellegrini *et al.*, "Initial measurements of the UCLA RF photoinjector," *Nucl. Instrum. Meth. A*, vol. 340, pp. 219-230, February 1994.

[11.56] S. Skelton. (2007). *Multi-quadrupole scan for emittance determination at PITZ* [Online]. Available FTP: www-zeuthen.desy.de Directory: students/2007/doc File: skelton.pdf

[11.57] The lattice of the FLASH injector beam diagnostics section to measure the emittance and the Twiss parameters was designed by P. Piot, Fermilab: the code to calculate the emittance using the multi-screen method is based on a similar code provided to us by P. Emma, SLAC.

[11.58] M. Geitz, "Investigation of the transverse and longitudinal beam parameters at the TESLA test facility linac," Ph.D. Thesis, Universität Hamburg, Hamburg, Germany, 1999.

[11.59] J. J. Scheins, "Tomographic reconstruction of transverse and longitudinal phase space distributions using the maximum entropy algorithm," TESLA Technology Collaboration, Technical Report No. 2004-08, May 2004.

[11.60] G. Minerbo, "MENT: A maximum entropy algorithm for reconstructing a source from projection data," *Computer. Graph. Image Process.*, vol. 10, pp. 48-68, May 1979.

[11.61] G. N. Minerbo, O. R. Sander and R. A. Jameson, "Four-dimensional beam tomography," *IEEE Trans. Nucl. Sci.*, vol. 28, pp. 2231-2233, June 1981.

[11.62] C. T. Mottershead, "Maximum entropy beam diagnostic tomography," *IEEE Trans. Nucl. Sci.*, vol. 32, pp. 1970-1972, October 1985.

[11.63] M. Röhrs, C. Gerth, H. Schlarb *et al.*, "Time-resolved electron beam phase space tomography at a soft x-ray free-electron laser," *Phys. Rev. ST Accel. Beams*, vol. 12, pp. 050704-1–050704-13, May 2009.

[11.64] M. Röhrs, C. Gerth, H. Schlarb *et al.*, "Time-resolved electron beam phase space tomography at a soft x-ray free-electron laser," *Phys. Rev. ST Accel. Beams*, vol. 12, pp. 050704-1–050704-13, May 2009.